SANDIA REPORT
SAND2006-0654
Unlimited Release
Printed January 2006

Separation and Concentration of Water-Borne Contaminants Utilizing Insulator-Based Dielectrophoresis

Blake A. Simmons, Eric B. Cummings, Rafael V. Davalos, Gregory J. Fiechtner, Blanca H. Lapizco-Encinas, Gregory J. McGraw, Allen J. Salmi, Joseph T. Ceremuga, Michael Kanouff, Yolanda Fintschenko

Prepared by
Sandia National Laboratories
Albuquerque, New Mexico 87185 and Livermore, California 94550

Sandia is a multiprogram laboratory operated by Sandia Corporation,
a Lockheed Martin Company, for the United States Department of Energy's
National Nuclear Security Administration under Contract DE-AC04-94-AL85000.

Issued by Sandia National Laboratories, operated for the United States Department of Energy by Sandia Corporation.

Available to DOE and DOE contractors from
U.S. Department of Energy
Office of Scientific and Technical Information
P.O. Box 62
Oak Ridge, TN 37831

Telephone: (865) 576-8401
Facsimile: (865) 576-5728
E-Mail: reports@adonis.osti.gov
Online ordering: http://www.doe.gov/bridge

Available to the public from
U.S. Department of Commerce
National Technical Information Service
5285 Port Royal Rd
Springfield, VA 22161

Telephone: (800) 553-6847
Facsimile: (703) 605-6900
E-Mail: orders@ntis.fedworld.gov
Online order: http://www.ntis.gov/help/ordermethods.asp?loc=7-4-0#online

SAND2006-0654
Unlimited Release
Printed January 2006

Separation and Concentration of Water-Borne Contaminants Utilizing Insulator-Based Dielectrophoresis

Blake A. Simmons, Eric B. Cummings, Rafael V. Davalos, Gregory J. Fiechtner, Blanca H. Lapizco-Encinas, Gregory J. McGraw, Allen J. Salmi, Joseph T. Ceremuga, Michael Kanouff, Yolanda Fintschenko

Sandia National Laboratories
Livermore, California 94551

Abstract

This report focuses on and presents the capabilities of insulator-based dielectrophoresis (iDEP) microdevices for the concentration and removal of water-borne bacteria, spores and inert particles. The dielectrophoretic behavior exhibited by the different particles of interest (both biological and inert) in each of these systems was observed to be a function of both the applied electric field and the characteristics of the particle, such as size, shape, and conductivity. The results obtained illustrate the potential of glass and polymer-based iDEP devices to act as a concentrator for a front-end device with significant homeland security and industrial applications for the threat analysis of bacteria, spores, and viruses. We observed that the polymeric devices exhibit the same iDEP behavior and efficacy in the field of use as their glass counterparts, but with the added benefit of being easily mass fabricated and developed in a variety of multi-scale formats that will allow for the realization of a truly high-throughput device. These results also demonstrate that the operating characteristics of the device can be tailored through the device fabrication technique utilized and the magnitude of the electric field gradient created within the insulating structures. We have developed systems capable of handling numerous flow rates and sample volume requirements, and have produced a deployable system suitable for use in any laboratory, industrial, or clinical setting.

This page intentionally left blank

Contents

Figures

This page intentionally left blank

1. Introduction

1.1 Background of Dielectrophoresis

Dielectrophoresis (DEP), a phenomenon first described by Pohl in 1951, is the movement of particles caused by polarization effects in a nonuniform electric field[1, 2]. DEP can take place in either direct (DC) or alternating (AC) electric fields[3]. Any dipole (permanent or induced) will have a finite separation between equal amounts of positive and negative charges. The dipole will align with the electric field, but if the electric field is nonuniform, one side of the dipole will be in a region with a lower field intensity than the other. This will produce an uneven charge alignment in the particle; i.e., uneven charge density in the particle; and inducing it to move toward the regions of greater field strength.[4, 5] If the effective polarizability of the particle is greater than that of the medium then the particle will exhibit positive dielectrophoretic behavior since it will be attracted to regions of greater field intensity. Negative dielectrophoretic behavior or repulsion from regions of greater electric field intensity, is observed in particles with lower polarizability than that of the medium.[4, 5]

DEP is of second order in the applied electric field. Electrokinesis is of first order in the applied electric field. At low applied electric fields, DEP is negligible when compared to electrokinesis. There are two regimes of DEP, the first regime, "streaming dielectrophoresis," occurs when DEP overcomes diffusion, but does not overcome electrokinetic flow. Under streaming DEP the particles flow along streamlines. The second DEP regime is called "trapping dielectrophoresis." Trapping DEP occurs when DEP overcomes diffusion and electrokinesis. Under this regime, particles are dielectrophoretically immobilized and can be significantly concentrated, nearly to solid density.[6] A comprehensive study comparing streaming and trapping DEP was recently reported by Cummings and Singh.[6]

The first studies utilizing DEP to manipulate cells employed electrodes of different shapes in order to produce nonuniform electric fields. Pohl et al.[4, 7, 8] used pin-plate and pin-pin electrodes to separate live and dead yeast cells and achieved collection of yeast cells on the electrodes. Recently, due to the availability of micro-fabrication techniques, DEP applications have been carried out using arrays of microelectrodes and AC electric fields. The minute dimensions of microelectrodes permit decreased space between electrodes, generating higher electric field intensity, which leads to greater DEP forces and minimized heating effects.[5, 9]

Markx et al.[10] characterized and separated yeast, gram positive, and gram negative bacteria by employing polynomial and interdigitated microelectrodes. They also achieved the separation of viable and non-viable yeast cells.[11] In 1996, Markx et al.[12] also carried out DEP separation of bacteria on interdigitated microelectrodes by varying the conductivity of the medium. Medoro et al.[13] developed a cell manipulator device based on programmable DEP-force cages by using 3D structures of electrodes. Particles were trapped, kept in levitation and dragged above the chip surface. This cell sensor/manipulator device was improved later[14, 15] by adding a more sophisticated software control over the DEP cage. Müller et al.[16] also developed a 3D microelectrode

system for the handling and the caging of single cells and particles. Their system consisted of two layers of electrodes separated by a flow channel, designed to trap eukaryotic cells (10-30 μm in diameter). Fiedler et al.[17] used a DEP microdevice that contained a 3D cage that was used to trap latex particles and cells. Li and Bashir[18] separated live and heat treated cells of *Listeria* on microfabricated interdigitated electrodes. The manipulation and separation of submicron particles, such as latex spheres and viruses, has also been reported.[19-26] Furthermore, the dielectrophoretic collection of protozoan parasites has been analyzed using DEP. Quinn et al.[27] collected *Cryptosporidium parvum* oocysts by re-circulating a suspension of oocysts through an electrode chamber by using a pump. The magnitude of the DEP collection of the oocysts was analyzed as function of ozone treatment given to the oocysts. It was found that the level of ozonization affected the outcome of the DEP experiments, since dead oocysts have a different DEP response than live oocysts.

Field-Flow Fractionation (FFF) has also been used for dielectrophoretic separation of cells. In DEP-FFF the particles are injected into a carrier fluid that passes through a separation chamber, and the separating force is applied perpendicular to the flow. Particles can be thus levitated at different heights from the chamber wall, reaching higher positions in the parabolic velocity profile of the liquid flowing through the chamber. Particles are eluted from the chamber in decreasing order of their velocities.[28, 29] Gascoyne's research group[30, 31] utilized a DEP-FFF system to separate mammalian cells. The cells were levitated inside the microchannel by using the DEP force. The cells' positions in the parabolic flow profile were controlled by using an interdigitated array of microelectrodes. Cells were eluted from the DEP-FFF system as function of the frequency and voltage of the applied electric field and their dielectric characteristics.

Several of the DEP studies mentioned above have used electrode chambers[4, 7, 8, 13-15, 18-26] to perform DEP studies. Usually the sample is introduced inside the electrode chamber, and the chamber is then closed and the electric field is applied. There is no liquid flowing through the chamber during the application of the electric field; i.e., there is no electrokinetic or pressure-driven flow opposing the dielectrophoretic trapping and therefore the trapping of particles or cells is less difficult. In other systems, liquid flow through the chamber is generated after the particles have trapped due to the DEP force, but not before or during the DEP trapping.[11, 12]

The large majority of the recent DEP studies reported have used thin-film electrode arrays (e.g. polynomial, interdigitated, sawtooth) fabricated in channels/flow cells with AC fields to generate nonuniform electric fields.[10-12, 18, 21-26, 30-33] Other studies have used three-dimensional electrode cages to capture and handle single cells and particles.[13-16, 19, 20] AC electric fields are used to eliminate electroosmosis and gas generation.[6] However, electrode-based DEP suffers from a number of drawbacks including the relative difficulty in fabricating devices with a robust thin-film electrode array and effects of charging the electrodes when operating at low frequencies.[34] In addition, electrodes foul, produce electrochemical changes in the liquid, and produce narrow zones of electric fields that can damage the cells or particles being manipulated. Electrode polarization effects can become highly problematic at low frequencies, producing a significant reduction in particle manipulation capabilities.[34] Moreover, conventional electrode designs are incompatible with the application of an electrokinesis-

driving voltage applied down a DEP system, therefore, in conventional DEP separations, the DEP force only competes with diffusion or advection. In addition, the typical device used for DEP studies is usually small due to the difficulties of making microelectrodes over large areas.[35]

The use of insulators rather than electrodes to produce a nonuniform electric field has a number of advantages. Insulators are less prone to fouling; i.e., they generally retain their function in spite of surface changes. Insulators are more robust and chemically inert than metallic electrodes. Fabrication with insulating materials is simpler since no metal evaporation or deposition is needed. Higher electric fields may be applied without the disadvantage of gas generation due to electrolysis at the metal electrodes. Designs using insulators instead of electrodes allow DEP to compete with electrokinetic or hydrodynamic flow, i.e. insulators open the possibility for flow-through systems. Insulator-based dielectrophoresis (iDEP) was first described by Cummings and Singh in 2000.[36] This method employs an array of insulating posts etched in a microchannel in order to create a non-uniform electric field. The posts are fabricated from an insulating material (e.g., glass or plastic). Only two electrodes are needed, at the solution inlet and outlet. The insulating posts act as obstacles to the electric field. The electric field between the two electrodes has to move around the insulating posts, creating zones with higher field strength (narrow zones between posts).[6, 36, 37]

Insulator-based dielectrophoresis has a great deal of promise for a number of reasons including the scalability of such structures to large volumes via massive parallelization. Insulators can be fabricated from plastic; the malleability of plastic facilitates the scale-up of DEP devices for high throughput operations. This has tremendous applications in the field of water analysis, where 1 L of water may have only 1 pathogenic bacterium. Thus, the need for selective concentration of cells is high. Methods such as filtration involve a lengthy culture step. By utilizing iDEP, selectivity and concentration could be accomplished in a single step. Whereas iDEP has been demonstrated with polystyrene beads and DNA[6, 36-38] it has not been demonstrated with live and dead bacteria cells.[34] There is a great potential for the application of iDEP for the separation, trapping, and concentration of bacteria from water. As mentioned above, iDEP is suitable for massive parallelization; therefore it is feasible to develop a high-throughput operation for water analysis based on DEP.

There are other techniques that allow fast separation and identification of microorganisms. One of these techniques is capillary electrophoresis (CE). A number of studies have been carried out using CE for the separation of bacteria and viruses [39-55]. In CE of microorganisms the intact microbes can be separated based on their characteristic charge to mass ratio. This characteristic charge varies with pH, solution composition, ionic strength and temperature[40]. Armstrong et al. [39-41, 43, 44, 52, 56] have performed a numbers of studies on CE and isoelectric focusing of microorganisms. In their studies they used a dissolved polymer to minimize the electroosmotic flow and high efficiencies were obtained, up to 850,000 plates/m for the bacteria *M. luteus*. In addition, the polymer employed seemed to produce some size and shape selectivity[39]. Their studies included the separation of the major pathogens in urinary tract infections[56], the separation of microbial aggregates[44] and the determination of cell viability for *B. infantis, L. acidophilus and S. cerevisiae*; where the results obtained did not show difference between the electrophoretic behavior of live and dead cells, since the

peaks of live and dead cells had essentially the same retention time[40]. In other report, the same retention time was also obtained for live and dead *L. acidophilus* cells from commercial tablets[41]. They have also observed that the addition of a small amount of polymer to the running buffer improves significantly the efficiency of the CE separation of microorganisms by producing focusing effects, but it is also necessary to carefully control other operating condition such as pH, buffer type, etc.[42, 43]

Other studies of CE of microorganisms discuss the importance of the double layer formed on the bacteria outer surface[46], surface properties[47] and the combination of CE of bacteria with immunofluorescent staining[48]. Continuous concentration of bacteria has been carried out using electrokinetic techniques such as zone electrophoresis and isoelectric focusing;[45] fine flow control has been achieved on a chip using electroosmosis and electrophoresis;[49] and surface characterization studies have been performed to analyze the dependence of electrophoretic mobility (μ_{EPH})on ionic strength.[53] The determination of the electrophoretic mobility of bacterial cells has been the focus of several studies. It has been found that the μ_{EPH} of bacteria depends on surface softness, structure and charge, cell age, as well as ionic concentration and pH of the running buffer.[50, 54, 55]

FFF is another alternative for bacterial separations, an excellent overview of the biological applications of FFF has been reported by Giddings.[57] FFF has also been used as a method for bacterial sample preparation prior to mass spectrometry analysis[58] and to separate selenium-laden cells from normal ones based on their size.[59] Nevertheless, iDEP has a main advantage over the other methods mentioned; iDEP can achieve very high sample concentration (almost to solid density)[6], since bacterial cells can be retained while the background liquid passes through the iDEP device.

Polymer microfluidic devices have been shown for several years in the fields of separation and other lab-on-a-chip applications. Unlike other microsystem fabrication platforms, polymer devices can be cheaply and reliably mass produced since they are highly compatible with mass commercial fabrication techniques such as injection molding and hot embossing. This publication focuses on and presents the capabilities of polymer-based iDEP devices for the concentration and removal of water-borne bacteria, spores and inert particles using our micro-iDEP device. We demonstrate that the device performance can be directly linked to the cross-sectional transverse profile presented by the insulating structures. The dielectrophoretic behavior exhibited by the different particles of interest (both biological and inert) in each of these systems was observed to be a function of both the applied electric field and the characteristics of the particle, such as size, shape, and conductivity. The results obtained illustrate the potential of polymer-based iDEP devices to act as a concentrator for a front-end device with significant homeland security applications for the threat analysis of bacteria, spores, and viruses. The polymeric devices exhibit the same iDEP behavior and efficacy in the field of use as their glass counterparts, but with the added benefit of being easily mass fabricated and developed in a variety of multi-scale formats that will allow for the realization of a truly high-throughput device. These results also demonstrate that the operating characteristics of the device can be tailored through the device fabrication technique utilized and the magnitude of the electric field gradient created within the insulating structures.

1.2 Theory of Dielectrophoresis

Described in Cummings and Singh [60] is a detailed description of the different regimes of DEP at DC fields. As stated in their publication [60], DEP has to overcome diffusion and EK flow (as well as pressure-driven flow if present) in order for the particles to be dielectrophoretically trapped by a DC electric field. The EK velocity, which is proportional to the electric field, comprises the effects of electroosmosis and electrophoresis [37]. The dielectrophoretic velocity, which is a second order effect of the electric field, can be expressed as [37]

$$\mathbf{u}_{DEP} = -\mu_{DEP}\nabla(\mathbf{E}\cdot\mathbf{E}), \tag{1}$$

where $\mathbf{u}_{DEP}$ is the dielectrophoretic velocity, μ_{DEP} is the dielectrophoretic mobility, and $\mathbf{E}$ is the electric field. For dilute, creeping flow in insulating, impermeable channels, the flux of particles, $\mathbf{j}$, including diffusion, pressure-driven flow, EK flow and DEP is [37]

$$\mathbf{j}\cdot\mathbf{n} = 0 \qquad \text{on the channel boundaries, and} \tag{2}$$

$$\mathbf{j} = -D\nabla C + C(\mathbf{u} + \mathbf{u}_{EK} + \mathbf{u}_{DEP}) \qquad \text{in the channel,} \tag{3}$$

where $\mathbf{n}$ is the normal to the surface, D is the diffusion coefficient, C is the concentration of particles, $\mathbf{u}$ is the velocity of the pressure-driven flow (non-electrokinetic component of the velocity).

The EK velocity ($\mathbf{u}_{EK}$) is related linearly to the electric field

$$\mathbf{u}_{EK} = \mu_{EK}\mathbf{E}, \tag{4}$$

Where

$$\mu_{EK} \equiv \mu_{EP} - \mu_{EO}, \tag{5}$$

defines the electrokinetic mobility from a superposition of the electrophoretic mobility and the electroosmotic mobility, μ_{EO}, of the opposing flow generated at the liquid/channel interface. Normally, immersed bacterial cells have a negative surface charge, thus μ_{EP} has the same sign as μ_{EO} when a substrate having a negative surface charge (e.g., glass) is employed. It is possible to obtain a simplified version of Equation (3) at trapping where the flux along the electric field lines is equal to zero ($\mathbf{j}\cdot\mathbf{E} = 0$) and for cases where diffusion and pressure-driven effects are negligible, the flow of particles is controlled by the electrokinetic and dielectrophoretic velocities

$$\mathbf{j}\cdot\mathbf{E} = 0 \approx C\left[(\mu_{EP} - \mu_{EO})\mathbf{E} - \mu_{DEP}\nabla I\right]\cdot\mathbf{E} \qquad \text{in the channel,} \tag{6}$$

where $I \equiv \mathbf{E}\cdot\mathbf{E}$ is the local field intensity.

Thus a condition for dielectrophoretic trapping in a given region is

$$\frac{\mathbf{u}_{DEP}\cdot\mathbf{u}_{EK}}{\mathbf{u}_{EK}\cdot\mathbf{u}_{EK}}=\frac{\mu_{DEP}}{(\mu_{EP}-\mu_{EO})}\frac{\nabla I}{I}\cdot\mathbf{E}>1 \tag{7}$$

Equation (7) shows that particles having a smaller μ_{EK} can be trapped at lower **E**. The DEP force acting on a spherical particle can be described by Equation (1)[2].

$$F_{DEP}=2\pi\varepsilon_0\varepsilon_m r^3 f(\tilde{\sigma}_p,\tilde{\sigma}_m)\nabla E^2 \tag{8}$$

where: ε_0 is the permittivity of free space, ε_m is the relative permittivity of the suspending medium, r is the radius of the particle, ∇E^2 defines the local field strength, $\tilde{\sigma}_p$ and $\tilde{\sigma}_m$ are the complex conductivities of the particle and the medium respectively, and $f(\tilde{\sigma}_p,\tilde{\sigma}_m)$ is known as the Clausius-Mossotti factor. At low frequency AC or DC electric fields, the dominant regime is the dielectric regime, for which the Clausius-Mossotti factor is defined as follows:[2, 61].

$$f(\tilde{\sigma}_p,\tilde{\sigma}_m)=\left[\frac{\tilde{\sigma}_p-\tilde{\sigma}_m}{\tilde{\sigma}_p+2\tilde{\sigma}_m}\right] \tag{9}$$

The complex conductivity is defined by Equation (3),

$$\tilde{\sigma}=\sigma+i\omega\in \tag{10}$$

where: $i=\sqrt{-1}$, and ω is the radian frequency of the applied electric field. For frequencies below 100 kHz or when DC electric fields are applied, the Clausius-Mossotti factor can be approximated in terms of the real conductivities as:[12, 62]

$$f(\tilde{\sigma}_p,\tilde{\sigma}_m)=\left[\frac{\sigma_p-\sigma_m}{\sigma_p+2\sigma_m}\right] \tag{11}$$

As it can be observed from Equation (8), the dielectrophoretic force acting on a particle can be positive or negative, depending on the sign of the Clausius-Mossotti factor. If the conductivity of the particle is greater than the conductivity of the medium, then the particle will exhibit positive DEP behavior, and vice versa. It has been reported that at low frequencies the applied electric field is primarily dropped across the outer cellular membrane, and the cells behave as poorly conductive spheres. At higher frequencies, the applied field is able to penetrate into the cells, and the cells behave as more conductive spheres having the conductivity of the cells interior[2, 10, 18, 29, 63-66]. Therefore, depending on the applied electric field (low-frequency AC, high-frequency AC or DC), different DEP responses can be present. In the current study only DC electric fields were used, therefore the DEP response of the cells depends essentially on the conductivity of the cellular membranes.

2. Experimental and Fabrication Details

2.1 Fabrication of Glass Devices

The microfluidic chip contains sets of independently addressable subcircuits. Each subcircuit is straddled by two liquid reservoirs and consists of separate patterned microchannels (Figure 1a). The length of the microchannels is 10.2 mm. Different post geometries were studied (squares, triangles and circles). The insulating posts transverse the entire depth of the microchannel (Figure 1b). The best results were obtained with microchannels with uniform square arrays of circular posts at different angles with respect to the applied electric field.

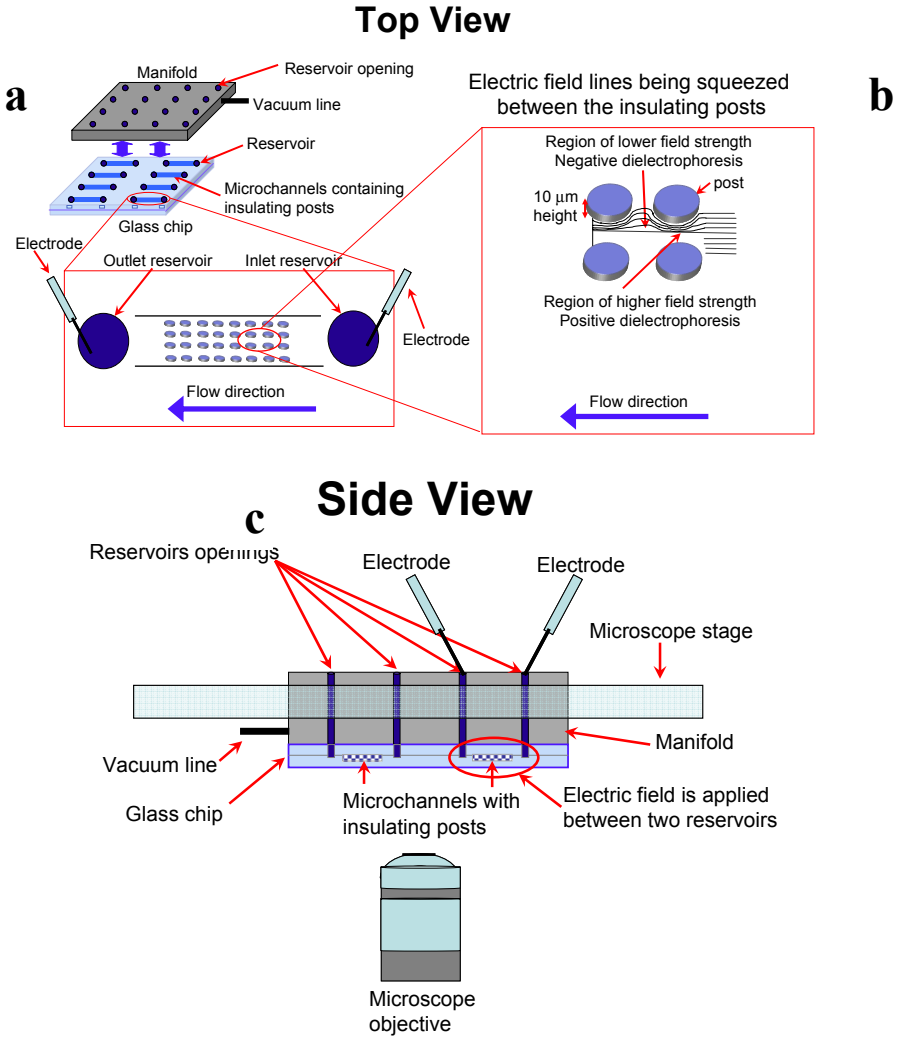

Figure 1. Schematic representation of the experimental set-up. (a) Top view, showing the manifold, glass chip , an enlargement of the flow microchannels; (b) cartoon showing the electric field lines being squeezed between the insulating posts; (c) side view showing the manifold and glass chip on the microscope stage. A similar setup was used for the polymer chip work, although the channel depth was greater than 10 μm, with the glass chip replaced with one made from a polymer.

The microchips were fabricated from Schott D263 glass wafers (100 mm diameter, 1.1 mm thickness, S. I. Howard Glass Company, Worcester, MA) using standard photolithography, wet etch, and bonding techniques. The photomasks were designed using DW-2000 (Design Workshop Technologies., Montreal, Canada) and Photo Sciences Inc., (Torrance, CA) generated the photomask. D263 borosilicate wafers were sputter deposited with chromium metal (Cooke Vacuum Products., South Norwalk, CT) 200 nm thickness, which served as the hard mask. A 7.5-μm thick layer of SJR 5740 (Shipley Corporation, Marlborough, MA) positive photoresist was spin-coated and soft-baked (90 ^{o}C, 5 minutes). The mask pattern was transferred to the photoresist by exposing it to UV light in a contact mask aligner at 775 mJ/cm^{2}.

Exposure time varied depending on flux intensity (MA6, Karl Suss America Inc., Waterbury Center, VA). After exposure, the photoresist was developed with Microposit developer concentrate (Shipley Corporation, Marlborough, MA) and hard-baked for 30 minutes at 125^{o}C. Exposed chromium was etched with CEN 300 Micro-chrome etchant (Microchrome Technologies Inc., San Jose, CA). The subsequently exposed glass was etched with a 16% HF solution (Shape Products Company, Oakland, CA). Via access holes were drilled in the cover plate (D263 Glass) with diamond-tipped drill bits (Amplex, Worcester, MA). The etched wafers and drilled cover plates were cleaned with 4:1 H_2SO_4:H_2O_2 (100^{o}C), de-stressed with 1% HF solution, then the surfaces were treated in 80^{o}C 40% NaOH, rinsed in a cascade bath, followed by a spin rinse dry, aligned for contacting, and thermally bonded by slowly ramping temperature to 610 ^{o}C for 5 hours in an N2-purged programmable muffle furnace (Model 48000, Thermolyne, Dubuque, IA). The standard chips were diced with a programmable radial arm saw (model 7100AD, Kulicke and Soffa., Willow Grove, PA) into individual devices.

2.2 Fabrication of Polymer Devices

Microfluidic channels were arranged on bonded discs of Zeonor 1060R resin (Zeon Chemicals, Tokyo, Japan). The lower discs were injection molded using a custom mold with a negative of the microchannel troughs and posts on its surface. The mold was fabricated using a glass or silicon master with the microchannel features photolithographically etched onto its surface. Since the mold is a negative of the master, the master and the final polymer disc contain the same features. The microchannels are arranged in 2 rows of 4 on each of the masters. Each microchannel was 10.2mm in length and 1mm wide. A rectangular array of insulating posts is placed in the center of the channel, 2.9mm from each end. Each disc featured two different array patterns, a 4x10 post array and a 5x12 post array. Only channels featuring the 4x10 array were used for the present dielectrophoresis experiments. The 4x10 array was composed circular posts with 200 μm diameters spaced 250 μm center-to-center. The rows at the front and back of the array featured a pointed surface facing outward to reduce fouling. Two distinct masters were produced using different standard etch techniques. In the first, a photolithographic pattern was defined on Schott D263 glass wafers and etched with hydrofluoric (HF) acid. This produced a stamp with characteristic Z-dimensions of 55 μm. The other fabrication process, a deep reactive ion etch (Bosch), was created by utilizing a different mask material patterned on a silicon wafer and produced 75 μm features.

After patterning, the masters were sputter coated with an electroplating base material, in this case 1500 Å of chrome (glass) or titanium (silicon) for adhesion promotion and 1500 Å of copper. The masters were then placed into a Digital Matrix commercial DM3M electroplating machine. The bath chemistry utilized was a standard nickel sulfamate with controlled pH to minimize stresses. Electroplating occurred at 48 °C for a total of 40 amp-hours and produced nickel films with thicknesses typically on the order of 1mm. The nickel was then planarized and machined to the set dimensions for use in our custom in-house fabrication facilities and the glass/silicon and metal seed layers dissolved. The nickel stamp was then thoroughly characterized through metrology, visual inspection, and electron microscopy.

Injection molding was carried out utilizing a 60-ton Nissei® (Nissei® America, Los Angeles, CA) TH-60 vertical injection molding machine. Pellets of Z1060R resin were dried at 40 °C for at least 24 hours before use. The resin was then fed to the machine through a gravity-assisted hopper connected externally to the injection molding barrel. Injection molding conditions were empirically determined by the operators, using the polymer supplier's recommendations as a starting point for molding. Cross-polarized optical interrogation of the replicated substrates was employed to assess and minimize residual stresses in the injection molded parts.

Premanufactured plaques of Zeonor® 1060R obtained from Zeon Chemicals (Louisville, KY) with a planar surface and a thickness of 1.5mm were used as the upper disc to seal the channel. Discs of the appropriate diameter were machined from the plaques to specified dimensions (typically ~80 mm). Through ports ("vias") of 1 mm diameter were drilled through the upper disc to provide a fluidic interface and reservoir at each end of the 8 microfluidic channels on the lower disc. The upper and lower discs were then thermally bonded using a Carver (Carver, Inc., Wabash, IN) press. Bonding conditions were held constant at the following: the press was heated to 190 °F with a constant applied load of 750 psi and a corresponding cycle time at temperature of 60 minutes. The bonded assembly was then cooled to 75 °F under constant load and then removed from the press. All bonded assemblies were checked for flow and channel blockage before use.

2.3 Apparatus

The manifold is ported with 16 openings spanning its thickness that coincide with the inlet and outlet vias of each channel. Each opening can accept a slip tip syringe and forms a watertight seal between the syringe and the drilled via. The channels were primed by gently forcing background solution through the channel with a syringe. Bubbles were removed with suction as necessary. After priming with DI water, 3ml slip tip syringes with plungers removed were loaded with approximately 1.5 ml of the desired tracer and inserted at the upstream and downstream ports of the manifold. The tracer was then gently forced into the channel with a plunger until the expected concentration of particles could be visualized. 0.508 mm diameter platinum-wire electrodes (Omega Engineering Inc., Stanford, CT) were inserted directly into the syringes. The positive electrode always corresponds to the upstream direction, since Zeonor® 1060R has a negative zeta potential at pH • 8. A programmable high voltage sequencer, Labsmith HVS 448 (Livermore, CA) was used to apply voltages of 1500V and below. A manually controlled power supply, Bertran ARB 30 (Valhalla, NY) was used for higher voltages.

The apparatus was visualized with an inverted epifluorescence microscope, model IX-70 (Olympus, Napa, CA). Different sets of fluorescence filters are employed: Chroma 51006, Chroma 51004 (Chroma Technologies Corp, Brattleboro, VT) and Olympus 41012 (Olympus, Napa, CA).

2.4 Sample Preparation

Lyophilized *Escherichia coli* (cell line BL21) was obtained from ATCC (Manassas, VA) and grown in LB nutrient broth. Cultures were grown overnight at 37 °C in an incubator to achieve saturation conditions. A 1:10 volumetric dilution of the cell culture were then allowed to grow in the LB liquid broth into late log phase to a cell concentration of 6 x 10^8 cells/mL, verified by OD measurements at 600 nm[67]. Cells were centrifuged at 5000 rpm for 10 minutes in order to eliminate the LB nutrient broth. Live cells were re-suspended in DI water utilizing a vortex mixer. Dead cells were obtained by heating an aliquot of live cells for 20 minutes at 80 °C. Live and dead cells were then labeled with the SYTO® 9-propidium iodide live/dead BAClight® bacterial stain (Molecular Probes, Inc., Eugene, OR) following the kit instructions. For live cells the SYTO® 9 labeling technique was utilized, whereas for the dead cells propidium iodide was used. This produces live cells that will fluoresce green (excitation/emission 480/500 nm) and dead cells that fluoresce red (excitation/emission 490/635 nm), and allowed for distinct direct visualization. For every mL of cell culture present in the vial containing the live cells, 3 μL of the SYTO® 9 green-fluorescent nucleic acid stain was added. For every mL of the dead cell culture, 3 μL of the propidium iodide staining solution was added. The cells were then incubated at room temperature for 15 minutes. Both cell types were then concentrated by centrifugation at 5000 rpm for 10 minutes. The labeled cells were recovered by centrifugation at 5000 rpm for 10 minutes, washed three times with DI water to remove any free dye, and finally re-suspended in DI water to the desired final volume to reach the appropriate cell concentration (typically 6 x 10^8 cells/mL). The DI water employed had a conductivity of 22.5 μS/cm, the conductivity meter employed was a Mettler Toledo MC126 (Mettler Toledo, Columbus OH). These two cell cultures were then mixed to give varying concentrations of live/dead cells. 50 μL of these cell cultures were added to the inlet reservoir in the flow manifold via pipette.

Bacillus subtilis (strain ATCC # 6633), *Bacillus cereus* (strain ATCC # 14579) and *Bacillus megaterium* (strain ATCC # 10778) were obtained from ATCC (Manassas, VA). Hydrodynamic diameters of the bacterial cells were estimated by dynamic light scattering (DLS) using a Zeta Plus Instrument (Brookhaven Instruments Corp., Holtsville, NY). In this technique the time-dependent fluctuations of scattered light intensity are measured to determine the translational diffusion constant of a suspended particle, which in turn can be related to the hydrodynamic diameter. The device was calibrating by using a solution of 200-nm polystyrene particles. The values of the hydrodynamic diameters of the bacterial cells are shown in Table 1. All cell types were grown in l Luria Bertani broth (LB). Cultures of the *Bacillus* species were grown at 30 °C in an incubator for 12 hours to achieve saturation conditions. A 1:20 volumetric dilution of each cell culture was then allowed to grow in the LB into late log phase to a cell concentration of 6 x 10^8 cells/ml, verified by OD measurements at 600 nm [67]. Cells were centrifuged at 5000 rpm for 10 minutes, in order to eliminate the LB, and re-suspended in DI water (pH 8) utilizing a vortex mixer. The cells were then labeled with Syto® 11 (green) or Syto® 17 (red)

bacterial stains (Molecular Probes, Inc., Eugene, OR). Syto® 11 and Syto® 17 produce cells that will fluoresce green (excitation/emission 508/527 nm) and red (excitation/emission 621/634 nm) respectively. For every milliliter of cell culture present in the vial, 3 μl of the fluorescent nucleic acid stain was added. The cells were then incubated at room temperature for 15 minutes. The labeled cells were recovered by centrifugation at 5000 rpm for 10 minutes, washed three times with DI water to remove any free dye, and finally re-suspended in DI water to the desired final volume to reach the desired cell concentration (typically 6 x 10^8 cells/ml). The labeled cell cultures were then used directly or mixed, and then 50 μl of this sample was added to the inlet reservoir in the flow manifold via pipette.

Table 1. Hydrodynamic diameters of the bacterial species utilized.

Species	Hydrodynamic diameter (μm)*	Flagella
E. coli	1.09 ± 0.32	Yes
B. subtilis	5.65 ± 1.23	No
B. cereus	4.01 ± 0.66	Yes
B. megaterium	3.15 ± 0.86	No

*Measured using light scattering.

Spore suspensions of *Bacillus subtilis* (strain ATCC # 6633) and *Bacillus thuringiensis* (strain ATCC # 29730) were obtained from Raven Biological Laboratories Inc. (Omaha, NE). The spore samples were labeled with Syto® 11 (Molecular Probes, Eugene, OR) dyes that labels the spores fluorescent green (excitation/emission 508/527 nm). The samples were dyed as received without any further modification. The spore samples were labeled by following the same protocol used with the vegetative bacterial cells. The final concentration of the labeled spores was 1x10^9 spores/ml.

2.5 Safety Considerations

The use of high voltage is a hazard that requires specific training and safety measures, such as interlocks and current-limiting features. All institutional requirements and safeguards were followed. The Syto® series labels were handled with care to prevent uncontrolled release and/or contamination by using containment protocols and appropriate personal protective equipment. All organisms used are considered Risk Group 1 and therefore pose no risk to healthy adult humans. Care was taken to handle all materials and dispose of the waste according to the US Center for Disease Control and Prevention (CDC) guidelines and Sandia National Laboratories' policies.

3. iDEP Device Performance: Glass

3.1 Separation of Gram-negative Bacteria and Polystyrene Particles

3.1.1 Electric Field Gradients with Insulating Posts

As it can be observed from Equation (1), the dielectrophoretic force is of second order in the applied electric field. By applying an electric field across a microchannel containing insulating posts, an electric field gradient is obtained as function of the post size and geometry.[6] Figure 1 shows the iDEP manifold and chip with a schematic representation of the electric field lines being squeezed between the insulating posts shown in Figure 1b. Figure 2 shows the variation of the dimensionless electric field intensity (E^2) produced by the array of insulating posts. The values of E^2 illustrated in the figure were normalized by the field intensity (E^2) without the insulators. The peak concentration factor is ~3.02, i.e., the field intensity is increased by a factor of 3 by the presence of the insulating posts. As it can be observed from the figure, the electric field intensity is higher at the narrow spaces between the posts; this is similar to the schematic representation of the field lines shown in Figure 1b. The potential barrier between the posts traps the particles. The data presented in Figure 2 was obtained by employing a potential flow solver called "*Laplace*". The flow field is solved directly from the Laplace equation ($\nabla^2\phi=0$) governing the electric potential without solving the coupled momentum transport (Navier-Stokes) and Poisson equations. Detailed information about Laplace potential flow solver can be found in Cummings and Singh.[6]

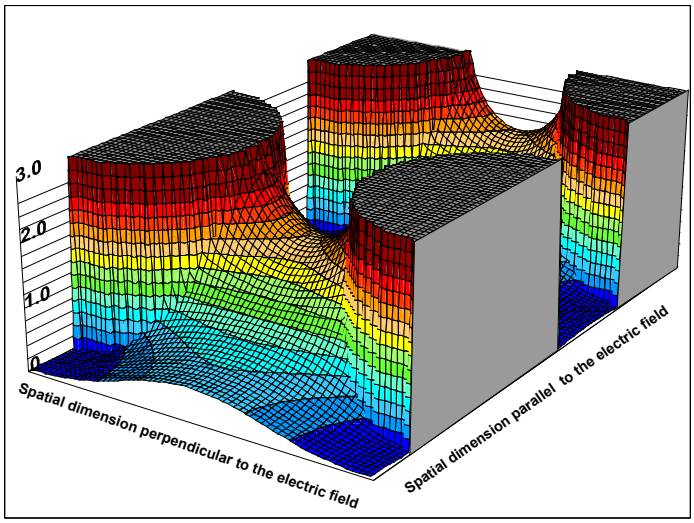

Figure 2. The variation of $||E||^2$, the electric field intensity, in an array of circular posts like in Figure 1b. The vertical axis shows the intensity normalized by the field intensity without the insulators. The peak concentration factor is ~3.02. By comparison, the theoretical field concentration factor for an individual circular post is 3. Flow direction is from left to right. The potential barrier between the posts traps the particles. The following post geometry was fed to *Laplace* potential flow solver: Circular posts are 130-μm in diameter, 200 μm center-to-center, and 0° offset.

3.1.2 Concentration of Viable *E. coli*

Figure 3 shows the concentration of live *E. coli*, a gram negative bacterium (stained in green color), obtained by applying iDEP. Figure 3a shows the cells in the microchannel filled with insulating posts (circular posts) before applying the electric field. In the absence of an electric field, the cells do not move. Figures 3b and 3c show the trapping of *E. coli* when a field of 120 V/mm and 160 V/mm are applied, respectively.

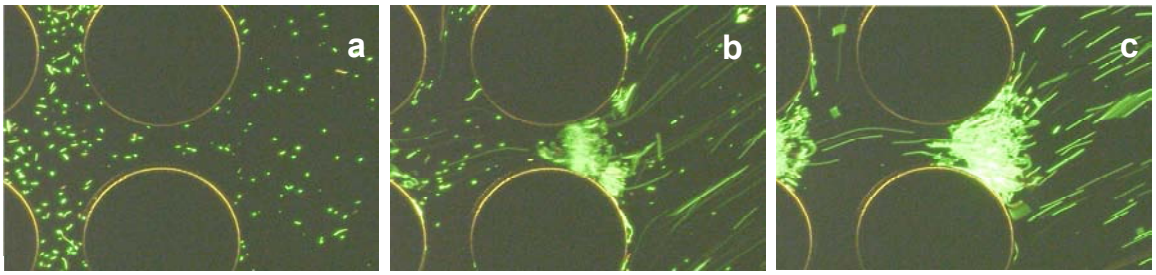

Figure 3. Concentration of live *E. coli* by using iDEP. 10 X magnification, inverted fluorescence microscope. Live *E. coli* cells are labeled green (Syto® 9 Molecular Probes, Eugene, OR) at a concentration of 6 x 10^7 cells/mL. Flow direction is from right to left. The background electrolyte was deionized water. The circular posts in the array have the following dimensions: 10-μm deep, 200-μm diameter, and 250 μm center-to-center, 0° offset, wet etched in glass. The electric fields were: (a) 0 V/mm no concentration of cells; (b) 120 V/mm, concentration of cells; and (c) 160 V/mm, high concentration of cells.

From the figures it can be noted *E. coli* is not trapped in the regions of higher field intensity (the narrowest space between the circular posts). At the lower electric field (120 V/mm, Fig. 3b) the cells are trapped closer to the region of higher field intensity. When the electric field is increased (160 V/mm, Fig 3c), the cells are more repelled from the region of higher field intensity. This indicates that under the current operating conditions live *E. coli* exhibits negative dielectrophoretic behavior. These results agree with the values of the Clausius-Mossotti factor shown in Table 2. The Clausius-Mossotti factor for the membrane of live *E. coli* cells is -0.5, which means that live *E. coli* is negative DEP under DC electric fields.

As mentioned above, under a DC electric field, the conductivity of the cell membrane is the dominant factor in the DEP behavior of the cells. The behavior shown in Figure 3c also illustrates the capability of iDEP for cell concentration, since a large amount of cells has been trapped in a small volume of the glass chip. As mentioned above, a sample of *E. coli* was introduced into inlet reservoir, and then a flow was generated by applying the electric field. The deionized water passed through the array of insulating posts, but the cells present in the water were retained between the posts due to the dielectrophoretic trapping. A quantitative cell concentration factor is not reported, due to limitations of the system setup. Qualitatively, it is possible to observe that the cells concentrate in a small region, because the brightness and the apparent area occupied by the cells increase.

Table 2. Conductivity of cell membranes and Clausius-Mossotti factors of cells suspended in DI water

Item	Conductivity (μS/cm)	Clausius-Mossotti factor (DI water as suspending medium)
Membrane of live cell[29]	1×10^{-3}	-0.50
Membrane of dead cell[28]	10	-0.23
Live *E. coli* cell[10]	412	+0.85
Polystyrene particles[68]	185	+0.71
DI water utilized*	22.5 ± 0.1	--

*Measurement performed with a Mettler Toledo MC126 conductivity meter.

3.1.3 Separation and Concentration of *E. coli* and Inert Polystyrene Particles

Because of the potential of iDEP as a front-end method for bacterial analysis in water, it was important to determine the behavior of *E. coli* in the presence of inert, non-cellular particles of similar size to the bacteria that could be in a sample background. Therefore, the behavior of bacteria with DEP was evaluated in the presence of polystyrene particles. The images obtained by applying iDEP to live *E. coli* and 1-μm rhodamine-labeled polystyrene particles (shown in red color) are presented in Figure 4. Figure 4a shows the cells and particles before the electric field had been applied. Figure 4b shows the DEP the response when an electric field of 200 V/mm is applied. From this figure it can be observed that the polystyrene particles exhibit a positive dielectrophoretic behavior, since they are trapped closer to the region of higher field intensity. Whereas, live *E. coli* is immobilized in areas where the electric field is less concentrated. Figure 4c shows differential DEP trapping of dead cells and 1-μm carboxilated-modified particles when a field of 40 V/mm is applied.; the carboxilated-modified particles exhibited positive DEP behavior while the dead cells exhibit negative DEP behavior. It has to be noted that the cells in Figures 4b (live cells) and 4c (dead cells) are being repulsed from the regions of higher field intensity, since the inert particles are positive DEP and the cells are negative DEP. These results are in agreement with the values of Clausius-Mossotti factors shown in Table 1 for the membrane of live cells and inert polystyrene particles. Thus, differential trapping of cells and particles has been achieved. This makes evident the potential of iDEP for cells/particle discrimination and concentration.

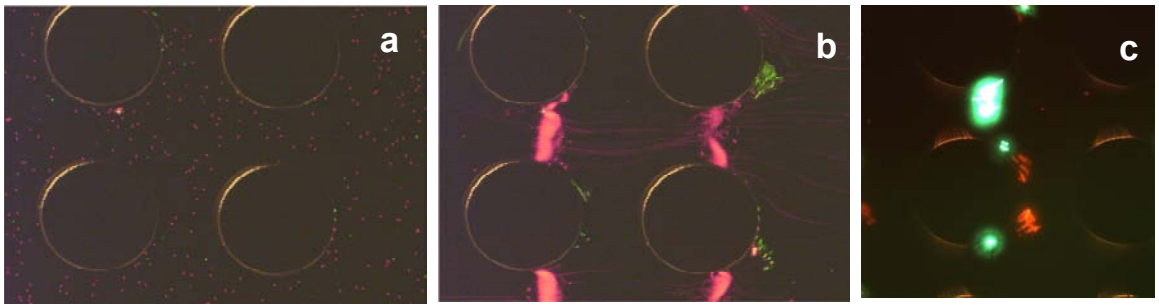

Figure 4. Simultaneous concentration and separation of live *E. coli* (green) and inert 1-μm red carboxylate-modified particles; and dead E. coli (red) and Inert 1-μm green carboxylate-modified particles by using iDEP. All conditions were as in Figure 3 except live cells were at a concentration of 6 x 10^6 cells/mL while the 1-μm polystyrene beads were at a concentration of 3.6 x 10^9 beads/mL. The circular posts in (a) and (b) have the following dimensions: 10-μm deep, 150-μm diameter, and 250 μm center-to-center, 0° offset, for (c) the center-to-center dimension is 200 μm. The electric fields applied were: (a) 0 V/mm, no DEP concentration of live cells or particles; (b) 200 V/mm, high concentration and differential trapping of cells (negative dielectrophoresis) and particles (positive dielectrophoresis); and (c) 40 V/cm, differential DEP trapping of dead cells and carboxylate-modified particles; particles exhibited positive DEP behavior while the dead cells exhibit negative DEP behavior.

Figure 5 presents the results obtained when a mixture of live *E. coli* and 200-nm inert rhodamine-labeled polystyrene particles was introduced into the system. Shown in Figure 5a is the response obtained when an electric field of 200 V/mm was applied. As observed in Figure 5a, a significant amount of the *E. coli* was trapped at the first row of insulating posts. Once the DEP traps at the first row were saturated, some cells leaked and were trapped at the second and third rows. In addition, due to the small size of the 200-nm inert particles, they are not immobilized by dielectrophoresis at the applied electric field (200 V/mm). From Equation (8) it can be noted the dielectrophoretic force acting on particle depends on the size of the particle, the larger the particle, the greater the DEP force. Therefore, for particles as small as 200-nm in diameter, higher applied electric fields are required to trap them under the current operating conditions. Figure 5b shows the release of live *E. coli* when the electric field of 200 V/mm was removed, it can be seen that the trapping of the cells was due solely to the applied electric field in terms of DEP force. The electric field of 200 V/mm was re-applied after the release; these results are shown in Figure 5c. Live *E. coli* was trapped again when the electric field was reapplied. Due to the previous release, the cells were able to reach further positions into the array of insulating posts; i.e., cells were trapped in significant amounts in the second and third rows of insulating posts. While in Figure 5a, most of the trapping was observed only at the first row.

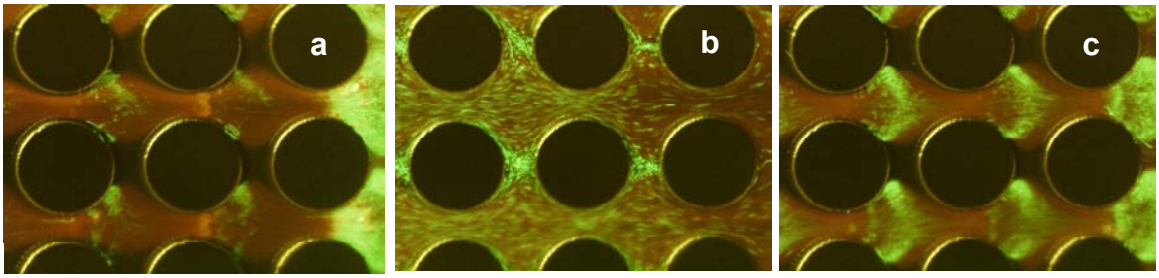

Figure 5. **Simultaneous concentration and separation of live *E. coli* and inert 200-nm red carboxylate-modified polystyrene particles by using iDEP. All conditions were as in Figure 3 except that 200-nm polystyrene beads were at a concentration of 4.6 x 10^{11} beads/mL. The circular posts in the array have the following dimensions: 10-μm deep, 120-μm diameter, and 200 μm center-to-center, 0° offset. The electric fields applied were: (a) 200 V/mm, high cell concentration and trapping at the first row of insulating posts, while 200-nm particles do not trap and exhibit streaming dielectrophoresis; (b) 0 V/mm release of *E. coli* cells from dielectrophoretic trapping; and (c) re-trap of cells at 200 V/mm, cells are re-trapped and concentrated at the first, second and third rows while 200-nm particles do not trap (streaming dielectrophoresis).**

From Figure 5c it can be observed that the cells trap in two distinct bands. The majority of the cells exhibit negative DEP behavior since they are trapped far from the areas of higher field strength. A small portion of the cells exhibit a less negative DEP behavior since they are trapped closer to the regions of higher field strength. It is believed that these latter cells were dead, and therefore, their DEP behavior changed. In order to prove this theory, a new set of experiments was carried out using live and dead cells that were labeled using a standard live/dead fluorescent assay.

3.1.4 Separation and Concentration of Viable and Dead *E. coli*

A mixture of live and dead *E. coli* was introduced into the system and differential trapping was observed. Figure 6 shows the results obtained with live and dead *E. coli*. The live cells are labeled with a green dye and the dead cells are labeled with a red dye. Figure 6a shows live cells exhibiting trapping DEP while dead cells exhibit streaming DEP at an applied field of 16 V/mm, at this low applied electric field only live cells are trapped while dead cells are able to pass through the array of insulating posts. From Table 1 it can be observed that the values of the Clausius-Mossotti factors for live and dead cells under a DC electric field are negative (values for the cell membrane). This means both, live and dead cells will exhibit negative DEP behavior. In addition, from Table 1, it can be seen that the magnitude of the Clausius-Mossotti factor for a live cell is greater than that of a dead cell. That is the reason why live cells are trapped at lower applied electric fields than dead cells. From Equation (1) it can be observed that the DEP force depends on the magnitude of the Clausius-Mossotti factor, the greater the magnitude of the Clausius-Mossotti factor, the greater the magnitude of the DEP force exerted on the particle. In this case, since live and dead cells are the same size, the different DEP behavior obtained between live and dead cells, is due to their different values of the Clausius-Mossotti factor. Figure 6b shows differential color-banding of the cells is

observed at an applied field of 40 V/mm. The dead cells are concentrated closer to the narrowest space between the posts and the live cells are concentrated closer to the wider area between the posts. By increasing the applied electric field to 60 V/mm (Figure 6c), it is possible to observe two separated bands of trapped cells. A red band, made up from the dead cells and a green band formed by the live cells. These results show true separation between live and dead cells. As for the few green cells present in the red band, it is believed that those cells are not viable, but since they were present in the sample of live cells, they are labeled green. From this figure, it can be observed that the band of dead cells is trapped in regions of higher field intensity, closer to the narrowest spaces between the circular posts. The live cells maintain the same negative dielectrophoretic behavior observed previously. From these results it can be stated that *the dead cells are less negatively dielectrophoretic than live cells*. The results are consistent with values of Clausius-Mossotti factors shown in Table 1; dead cells are less negatively dielectrophoretic than live cells due to the differences between their cell membrane conductivities (~10^{-3} S/m and ~10^{-7} S/m for dead and live cell membranes, respectively).[29]

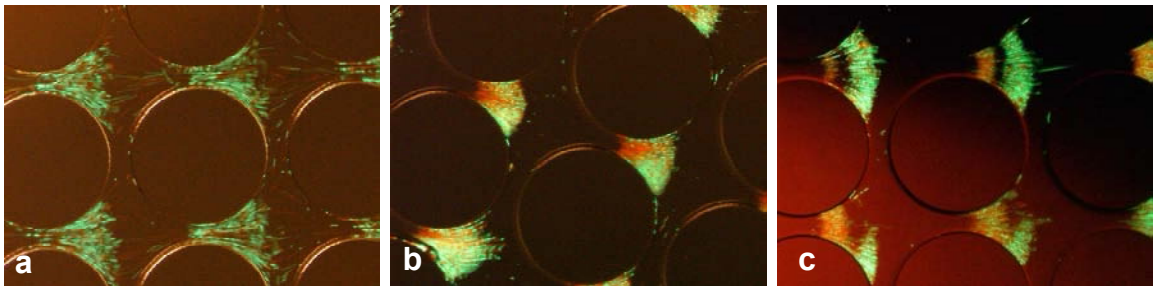

Figure 6. **Simultaneous concentration and separation of live (green) and dead (red) *E. coli* by using iDEP. All conditions were as in Figure 3 except that dead cells were at a concentration of 6 x 10^7 cells/mL and labeled with propidium iodide (red dye, Molecular Probes, Eugene, OR). The circular posts in the arrays have the following dimensions: 10-μm deep, 200-μm diameter, and 250 μm center-to-center, 0° offset in (a) and (c), and 20° offset in (b). The electric fields applied were: (a) 16 V/mm, only live cells are trapped, while dead cells exhibit streaming dielectrophoresis; (b) 40 V/mm, differential banding on live and dead cells is observed; and (c) 60 V/mm, differential trapping of live and dead cells is shown by two separate bands of different color, live cells (green) are trapped at the wider regions between the circular posts (negative dielectrophoresis) and dead cells (red) are less negatively DEP since they are trapped at the narrower regions between the circular posts.**

Since a DC electric field was applied in these experiments, the conductivity of the cell membrane was the dominant factor determining the DEP response of the cells. A dead cell membrane is expected to have a higher conductivity than a live cell membrane.[29] As discussed above, when a cell dies, the cell membrane becomes permeable and its conductivity is increased significantly. Therefore, by having a more conducting cell membrane, dead cells are less negatively dielectrophoretic than live cells. This differential dielectrophoretic behavior of live and dead cells is confirmed by the results presented in Figure 6c.

3.2 Differences between the Cell Surface of Gram-positive and Gram-negative Bacteria

Gram-positive and Gram-negative bacteria have different surface properties. Both types of bacteria have a cell membrane and a cell wall. Most bacteria have cell walls that give them shape and protect them from osmotic lysis [69]. The cell wall in Gram-positive bacteria consists of a thick layer of peptidoglycan (20–80 nm) and teichoic acids, which give the wall a negative charge. The Gram-negative cell wall is much more complicated, composed of an outer membrane (7–8 nm) and a thin layer of peptidoglycan (1–3 nm) [69, 70].

The cell membrane of both Gram-positive and Gram-negative bacteria is a lipid bilayer composed of phospholipids, glycolipds and proteins [70]. Cell membranes are thin (5–10 nm), and their main function is to retain the cytoplasm and serve as a permeable barrier. The membrane prevents the loss of essential components through leakage [69]. When the cell membrane has been compromised, the cytoplasm can leak out of the cell membrane increasing its conductivity [29, 71]. An intact cell membrane is a good insulator, being composed of lipids and proteins that present a simplified barrier to ions [35, 65]. The difference in conductivity between the cell wall and the cell membrane is significant; e.g., Suehiro *et al*. [71] have reported that the conductivities of the cell wall and cell membrane of *E. coli* are 5 x10^{2} μS/mm and 5 x 10^{-5} μS/mm respectively.

Since the cell wall is highly conductive, electric fields can easily pass through the cell wall. At low frequencies, however, the cell interior is shielded by the highly insulating cytoplasmic membrane; i.e., the membrane sustains the full electric potential applied to the cell [10, 29]. Burt *et al*., [65] state that at frequencies below 100 kHz, the low value of the bulk membrane conductivity prevents the applied electric field from penetrating the into the cytoplasm. As the frequency increases above 100 kHz, the membrane resistance is shunted by the membrane capacitance and the electric field is able to penetrate the cell [65].

These differences between Gram-positive and Gram-negative affect also the electrophoretic behavior of the cells [54]. Under physiological pH conditions both types of microorganisms have net negative charges [47, 53, 54]. Electrophoretic separations have been achieved between Gram-positive and Gram-negative bacteria [47, 54]. Sonohara *et al*. [54] found the Gram-negative bacterium *E. coli* to be charged more negatively and therefore to have a higher electrophoretic mobility (by a factor of 2) than the Gram-positive *Staphylococcus aureus*. In a similar study, Buszewski *et al*. [47] also reported higher electrophoretic mobilities (by a factor of 3) values for the Gram-negative bacterium *E. coli* than those for the Gram-positive bacterium *B. cereus*.

In the present study (performed at a pH of 8), the four species of bacterial cells, the Gram-negative *E. coli,* and the Gram-positive *B. subtilis*, *B. cereus* and *B. megaterium* all were observed to have indistinguishable electrokinetic velocities, meaning that electroosmosis dominated over electrophoresis. In other words, the impact of the differences in μ_{EP} on the overall μ_{EK} of each bacterial species was negligible. According to the studies reported by Buszewski *et al*. [47] and Sonohara *et al*. [54], the four species

of bacteria have μ_{EP} opposed to the EOF when using a substrate with a negative surface charge (e.g. glass). Since *E. coli* is Gram-negative, it has a higher density of negative charges on its membrane than the three Gram-positive *Bacillus* species and therefore has the most negative μ_{EP}. The overall EK mobility (μ_{EK}) of *E. coli* is therefore the lowest of the bacteria and consequently, in accordance with Equation (6), *E. coli* should exhibit iDEP trapping at lower dielectrophoretic velocities than the three *Bacillus* species. However, since the EK velocities of the four species of bacteria are indistinguishable, the effect of differences in μ_{EP} on the trapping behavior is likewise negligible.

Other published results confirm that the electrophoretic mobilities of bacteria are relatively low. Buszewski *et al*. [47] found the μ_{EK} of *E. coli* did not differ much from the μ_{EO}. Armstrong and He [40] carried out CE of live and dead bacteria, and their results showed no significant difference between the migration times for the live and dead bacteria. Li and Harrison [49] mentioned that in uncoated glass, the EOF is greater than the μ_{EP} of cells. Armstrong's research group has accomplished the separation of bacteria using CE and capillary isoelectric focusing by adding a polymer to the running buffer [39, 41, 43, 44]. Armstrong *et al*. [39] stated that without the addition of the polymer in the CE experiments, the microbes will elute near the EOF.

Thus, two major forces dominating the dielectrophoretic behavior of the bacteria in our system were drag from the EOF and the dielectrophoretic force. In order to trap dielectrophoretically, the condition simplifies somewhat to

$$\frac{\mu_{DEP}}{\mu_{EO}}\left(\frac{\nabla I}{I}\right)\cdot \mathbf{E} > 1 . \qquad (12)$$

The bacteria strain specificity arises from differences in dielectrophoretic mobility, which are dominated by factors other than electrical properties in these DC experiments as discussed below.

3.3 Separation of Gram-positive and Gram-negative Bacteria

Measurements of the lowest electric field applied required to achieve trapping were made for each bacterial species. In these experiments, only one bacterial species was used at a time. The goal of these experiments is to establish a trapping order or trend based on the minimum electric field required to achieve trapping. Sets of experiments were performed using two different solution conductivities: 2.2 and 10.4 μS/mm. The use of different solution conductivities helped to identify the mechanism of species specificity. If the membrane conductivity is the parameter controlling specificity, then increasing the medium conductivity should reduce specificity by reducing the relative differences in the CM factor. However, if the membrane conductivities are all much smaller than the medium conductivity, the CM factors of all species approach −0.5 regardless of the differences in conductivity and the species specificity cannot arise from electrical properties. Thus, if species specificity is observed *not* to change with solution conductivity, one can attribute specificity in these experiments to geometrical differences or other factors not included in conventional treatments of DEP. Based on the cell

membrane conductivity of 5 x10^{-5} μS/mm [71] of *E. coli* the CM factor in these experiments is practically equal to –0.5. In order to observe differential dielectrophoretic effects arising from differences in membrane conductivity, the other bacteria must have at least four orders of magnitude greater membrane conductivity than the *E. coli*, an unlikely difference that can be easily ruled out by repeating experiments at two different solution conductivities.

In order to monitor the minimum applied electric field required for DEP trapping, the bacteria sample was introduced into the microchannel and the electric field was increased until the bacteria began to be trapped. The results obtained are presented in Figure 7.

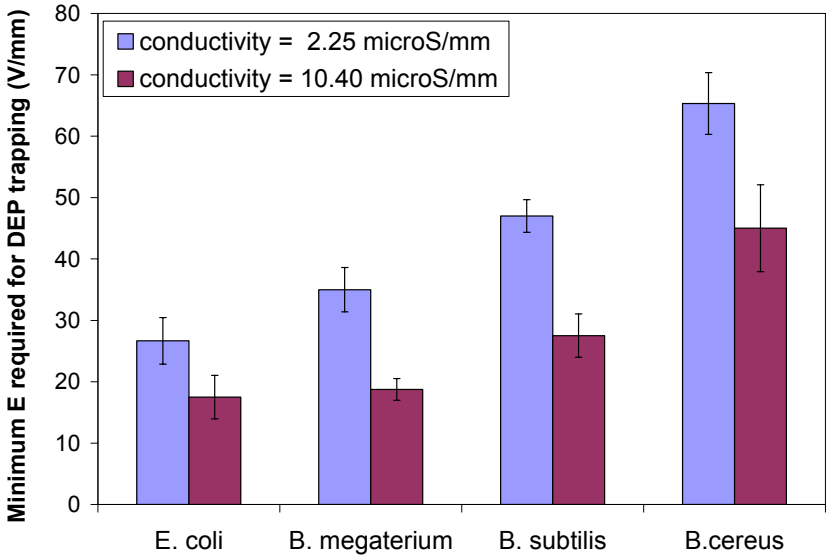

Figure 7. Minimum mean electric field required to achieve DEP trapping in the glass device that with 200 μm diameter posts with 250 μm center-to-center distances with a depth of 10 μm.

From Figure 7, it is observed that the order of trapping of the four species of bacteria, from the lowest to the highest electric field required, is as follows: *E coli* < *B. megaterium*< *B. subtilis* < *B. cereus.* The same order of trapping is observed at both values of solution conductivity, but lower applied electric fields are required when using the 10.4 μS/mm solution. The differences between the cell membrane conductivities are not sufficient to account for the differences in the electrophoretic behavior between the bacterial cells. These results demonstrate that parameters other than the electrical properties of the cell control the differences in dielectrophoretic response of the bacterial cells. These parameters include the cell size, shape, morphological characteristics and surface charge. In the case of surface charge, this parameter is directly related to the electrophoretic mobility of the cells, which, as discussed in the introduction, was not a significant factor in our experiments due to the presence of the EOF. If the EOF had been suppressed or eliminated, then the electrophoretic mobility would have been a significant parameter affecting the DEP trapping of the cells.

These results are different from those obtained in our first dielectrophoretic study of bacterial cells presented above [72]. The live and dead *E. coli* cells had essentially the same size, shape, morphological characteristics, electrokinetic mobility etc. The only significant difference between live and dead *E. coli* was the conductivity of the cell membrane, since dead cells, having compromised membranes, have a higher conductivity than live cells by ~4 orders of magnitude [29].

The results in Figure 7 indicate that *E. coli* exhibits the strongest negative DEP behavior, since DEP trapping of *E. coli* was obtained with the lowest applied electric fields. *B. cereus* exhibited the least negative dielectrophoretic behavior, since the highest applied electric fields were necessary to achieve DEP trapping. This trend is not in agreement with the relative size of the bacteria (Table 1). According to Eq. 6, derived for spherical particles, the DEP force scales with the volume of a particle. The drag force exerted by the EOF scales with the particle size. Thus, generally it is expected that lower applied electric fields are needed to trap larger particles, other things being equal. However, Figure 7 reinforces that *E. coli* have both the smallest size and strongest DEP behavior. Both the drag and dielectrophoretic forces depend on details of the particle shape. The long flagella of the *E. coli* and differing shapes of the species of bacteria are probably responsible for the poor agreement with the predictions of the simple sphere model used, but further studies are needed.

Figure 7 also illustrates the potential for the separation and concentration of different species of bacteria simultaneously. It is possible to concentrate a sample of different species of bacteria by applying a sufficiently high electric field to collect bacteria. Then each concentrated bacterial species can be selectively eluted by reducing the applied electric field in the manner of a conventional gradient elution.

3.3.1 Separation of *E. coli* and *B. subtilis*

Figure 8 shows the dielectrophoretic behavior observed when a mixture of equal amounts of *E. coli* (green) and *B. subtilis* (red) was introduced into the microchannel. *E coli* was stained green using Syto® 11 and *B. subtilis* was stained red using Syto® 17. In Figure 8a, when a lower electric field was applied (50 V/mm), mainly *E. coli* was trapped while *B. subtilis* flowed through the array of posts without trapping. In Figure 8b, at a higher electric field (75 V/mm) it was possible to trap both species of bacteria in spatially separate bands. As expected, both bacteria exhibited negative dielectrophoretic behavior since trapping occurred upstream of the area where the field is most concentrated. The band of *B. subtilis* is located closer to the peak electric field concentration (see Fig. 1) than the band of *E. coli*. Thus, *E. coli* (green band) exhibited greater negative dielectrophoretic mobility than *B. subtilis* (red band). These results agree with the trend presented in Figure 7, where *E. coli* is shown to trap at a lower applied electric field than *B. subtilis*.

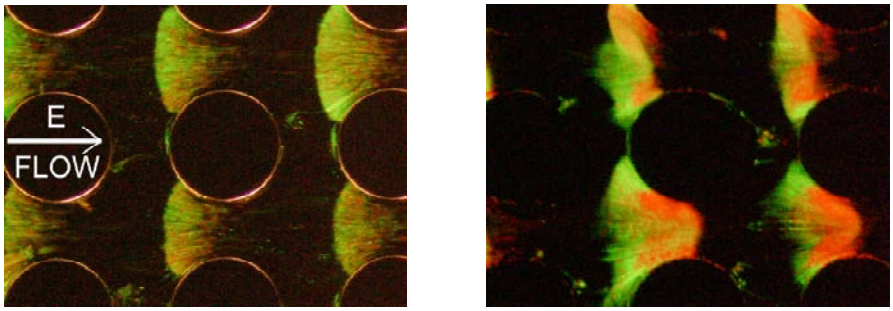

(a) 50 V/mm (b) 75 V/mm

Figure 8. Epifluorescence image of selective trapping of *E. coli* and *B. subtilis*. The inlet cell concentration is 3×10^8 cells/ml. *E. coli* and *B. subtilis* cells are respectively labeled green (Syto® 11) and red (Syto® 17). The flow direction is from left to right. The background electrolyte is deionized water whose pH has been adjusted to 8 by adding NaOH, and conductivity has been adjusted to 2.2 μS/mm by adding KCl. The circular posts in the flow-aligned square array are wet etched in glass 10-μm tall, 150-μm in diameter, and on 200-μm centers. The mean applied electric fields are: (a) 50 V/mm and (b) 75 V/mm.

The experiment was repeated using *E. coli* stained red with (Syto® 17) and *B. subtilis* stained in green (Syto® 11), and the same results were produced, i.e., *E. coli* exhibited a more negative dielectrophoretic mobility than *B. subtilis*. This set of experiments was done in order to verify the assumption that the DNA-intercalating dyes were not affecting the dielectrophoretic or electrokinetic behavior of the bacteria.

3.3.2 Separation of *E. coli* and *B. cereus*

The dielectrophoretic separation and concentration of *E. coli* (green) and *B. cereus* (red) are shown in Figure 9. The results are similar to those of Figure 8. At an applied electric field of 50 V/mm (Figure 9a), both cell species are trapped, but the majority of the trapped cells are *E coli.* By increasing the applied electric field to 75 V/mm (Figure 9b) it was possible to trap both species of bacteria in separate bands. *E. coli* exhibited a more negative dielectrophoretic mobility than *B. cereus* since it was trapped further upstream of the peak field concentration. These results are in agreement with the trend shown in Figure 7.

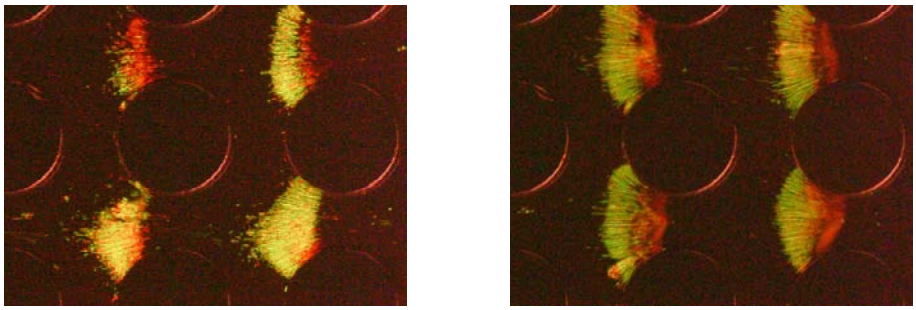

(a) 30 V/mm (b) 75 V/mm

Figure 9. Epifluorescence image of selective trapping of *E. coli* and *B. cereus*. All conditions are as in Figure 8 unless otherwise stated. *E. coli* and *B. cereus* cells are respectively labeled green (Syto® 11) and red (Syto® 17). The mean applied electric fields are: (a) 30 V/mm and (b) 75V/mm.

3.3.3 Separation of *E. coli* and *B. megaterium*

The dielectrophoretic separation and concentration of *E. coli* (green) and *B. cereus* (red) are shown in Figure 10. At an applied field of 50 V/mm (Figure 10a) *B. megaterium* flowed while *E. coli* are trapped. When the electric field was increased to 90 V/mm (Figure 10b) both types of bacteria were dielectrophoretically trapped. From the location of the bands of trapped bacteria, and the results in shown in Figure 7, it was shown that *E. coli* has a greater negative dielectrophoretic mobility than *B. megaterium*.

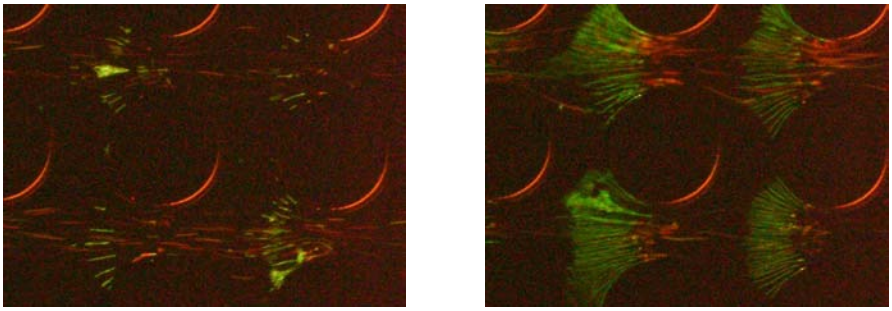

(a) 50 V/mm (b) 90 V/mm

Figure 10. Epifluorescence image of selective trapping of *E. coli* and *B. megaterium*. All conditions are as in Figure 8 unless otherwise stated. *E. coli* and *B. megaterium* cells are respectively labeled green (Syto® 11) and red (Syto® 17). The mean applied electric fields are: (a) 50 V/mm and (b) 90 V/mm.

3.3.4 Separation of *B. cereus* and *B. subtilis*

It was possible to selectively trap and concentrate a mixture of two *Bacillus* species. These results show that iDEP has potential for cell discrimination and identification, even when two different species of *Bacillus* are present. Figure 11a shows that at an applied field of 25 V/mm it was possible to selectively trap *B. subtilis* (red) while *B. cereus* (green) exhibited streaming DEP. At an electric field of 75 V/mm (Figure 11b), both

species of *Bacillus* were trapped. From the location of the bands of trapped bacteria it was found that *B. subtilis* has a greater negative dielectrophoretic mobility than *B. cereus*. This observation is consistent with the results in Figure 7.

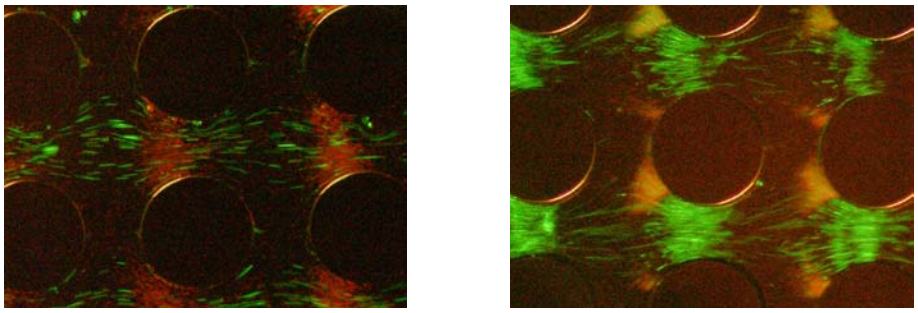

(a) 25 V/mm (b) 75 V/mm

Figure 11. Epifluorescence image of selective trapping of *B. subtilis* and *B. cereus*. All conditions are as in Figure 8 unless otherwise stated. *B. subtilis* and *B. cereus* cells are respectively labeled green (Syto® 11) and red (Syto® 17). The mean applied electric fields are: (a) 25 V/mm and (b) 75 V/mm.

3.3.5 Separation of *B. megaterium* and *B. subtilis*

In these experiments *B. megaterium* (green) and *B. subtilis* (red) were not able to be trapped in two spatially distinct bands. At an electric field of 50 V/ mm (Figure 12a), both bacteria are trapped. At a higher electric field of 75 V/mm (Figure 12b), both of the *Bacillus* species were dielectrophoretically trapped. The bands of bacteria, while offset, are not distinctly separated. From the location of the area of green cells, it can be said that *B. megaterium* on average exhibit a more negatively dielectrophoretic behavior than *B. subtilis*. Again, in agreement with Figure 7, *B. megaterium* exhibits a greater dielectrophoretic mobility than *B. subtilis*.

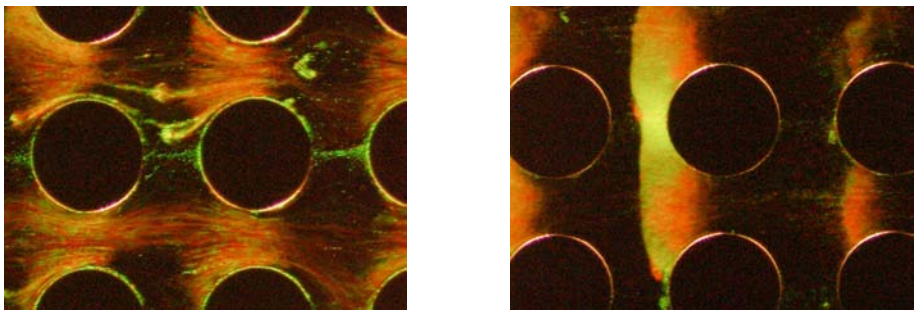

(a) 50 V/mm (b) 75 V/mm

Figure 12. Epifluorescence image of selective trapping of *B. megaterium* and *B. subtilis*. All conditions are as in Figure 8 unless otherwise stated. *B. megaterium* and *B. subtilis* cells are respectively labeled green (Syto® 11) and red (Syto® 17). The mean applied electric fields are: (a) 50 V/mm and (b) 75 V/mm.

3.3.6 Separation of *B. cereus* and *B. megaterium*

The selective concentration and separation between *B. cereus* (green) and *B. megaterium* (red) was observed at an applied electric field of 30 V/mm (Figure 13a). At this applied electric field, *B. megaterium* was dielectrophoretically trapped while *B. cereus* flowed through the array of posts. At a higher electric field of 75 V/mm (Figure 13b), both *Bacillus* species were dielectrophoretically trapped in spatially distinct bands. *B. megaterium* exhibited a greater negative dielectrophoretic mobility than *B. cereus*. In agreement with the trend shown in Figure 7, these results and are very encouraging, since they show that iDEP has the potential to clearly distinguish between different *Bacillus* species.

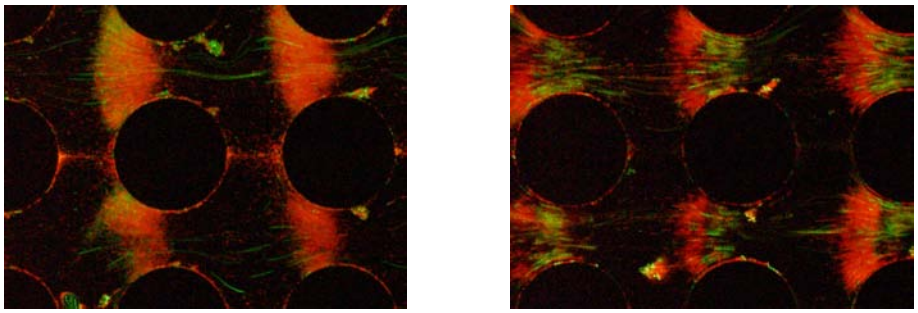

(a) 30 V/mm (b) 75 V/mm

Figure 13. Epifluorescence image of selective trapping of *B. cereus* and *B. megaterium*. All conditions are as in Figure 8 unless otherwise stated. *B. cereus* and *B. megaterium* cells are respectively labeled green (Syto® 11) and red (Syto® 17). The mean applied electric fields are: (a) 30 V/mm and (b) 75 V/mm.

3.4 Dielectrophoretic Separation of Spores

Spores are very important in water analysis since they are more resistant to traditional water treatments than vegetative forms of bacteria. Figure 14 shows the fluorescence of labeled *B. subtilis* spores collected in the iDEP device while a mean field of 200 V/mm was applied, showing a significant concentration effect. Figure 14b shows the release of the spores upon removal of the electric field, demonstrating the reversibility of dielectrophoretic trapping. We observed that the trapping threshold of spores is much higher than that of vegetative bacteria, allowing DEP to be used to separate vegetative cells and spores.

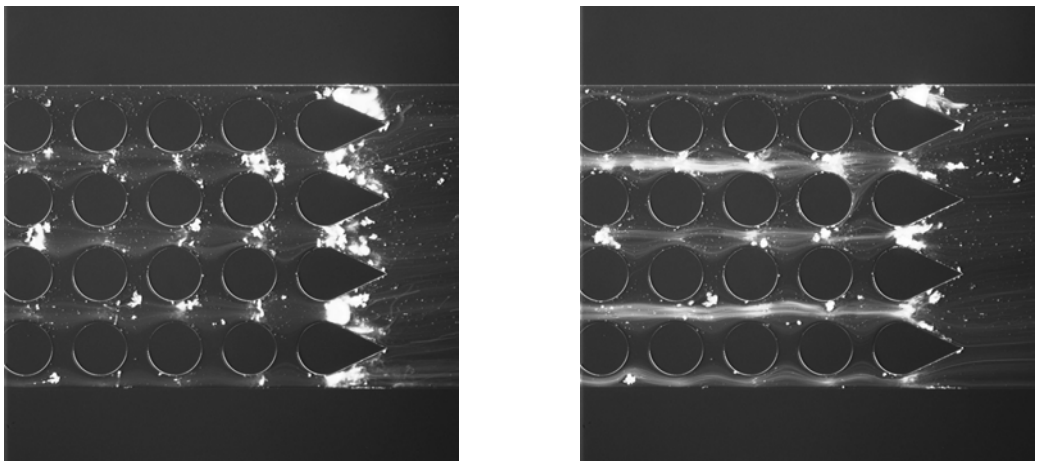

(a) (b)

Figure 14. Trapping and release of *B. subtilus* spores, 10X magnification. Spore concentration is 2 x 10^7 spores/ml. Spores are labeled green (Syto® 11). In this gray scale figure, spores appear white. Flow direction is from right to left. The background electrolyte is deionized water, pH=8, σ=20 μS/cm. The circular posts in the array are 10-μm tall, 200 μm in diameter, and on 250-μm centers. The mean applied electric field is 200 V/mm for (a) DEP trapping and (b) release.

3.5 Dielectrophoretic Separation of Viruses

The threshold for dielectrophoretic trapping and concentration of tobacco mosaic virus (TMV) was generally higher than that of spores and vegetative cells. Figure 15 shows the iDEP device collecting fluorescently labeled TMV at mean applied electric fields of 200 V/mm. Under these experimental conditions, TMV is observed to undergo negative dielectrophoresis. In order to test if the TMV could be selectively trapped against a more-concentrated background, experiments were performed in which a 20 μl sample of 200-nm fluorescently labeled red polystyrene beads at 1:100 dilution were added to the microchannel reservoirs along with the TMV sample.

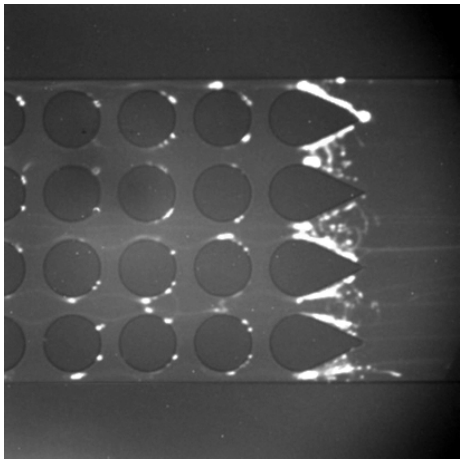

Figure 15. Trapping of TMV, 10X magnification. Virus concentration is 0.1 mg of virions/mL. TMV are labeled green (Syto® 11). In this gray-scale figure TMV appears white. Flow direction is from right to left. The background electrolyte is deionized water, pH=8, σ=20 μS/cm. The circular posts in the array are 10-μm tall, 200μm in diameter, and on 250-μm centers. The mean applied electric field is 200 V/mm.

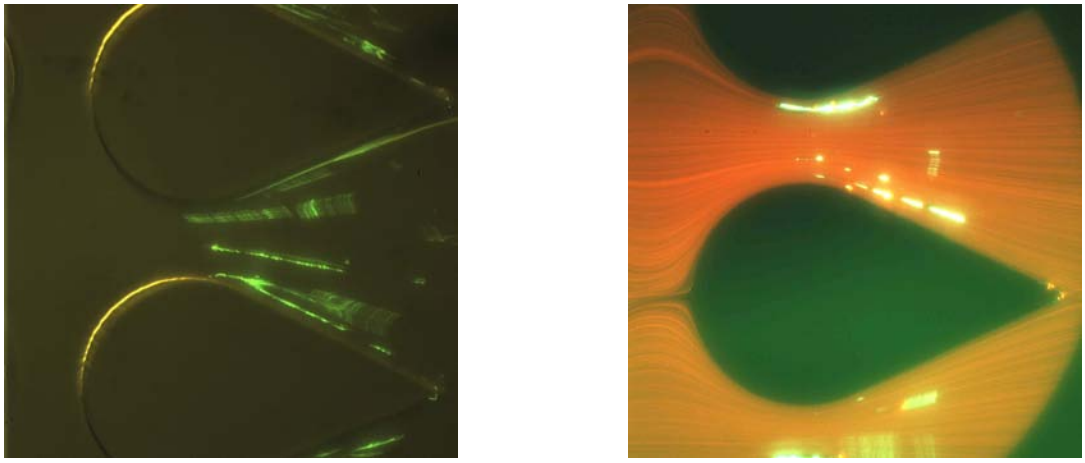

(a) (b)

Figure 16. Trapping of TMV under conditions as described in Figure 15, unless otherwise stated, 40X magnification: (a) TMV trapping between two posts at a mean applied field of 150 V/mm; (b) TMV trapping between two posts in the presence of 200-nm inter particles at a mean applied field of 100 V/mm. TMV is labeled green and the red background is provided by the presence of 200-nm polystyrene particles at 1:100 dilution.

Figure 16a shows details of TMV trapping between two posts at a mean electric field of 150 V/mm using a solution only containing TMV. Figure 16b shows details of TMV trapping in the presence of 200-nm, red-fluorescent, polystyrene particles at a mean applied electric field of 100 V/mm. The red 200-nm particles are not trapped at this

applied field. The electrokinetic mobilities of the beads and viruses were observed to be nearly identical, thus differences in the trapping behavior are dominated by differences in their dielectrophoretic behavior. These results again demonstrate that DEP can separate particles of similar sizes. Figure 17 plots the typical threshold mean applied DC electric fields to achieve dielectrophoretic trapping of the different microorganisms (bacteria, spores, viruses) in our iDEP device and our suspension liquid. The dielectrophoretic response of the microorganisms studied varies significantly, showing the potential of iDEP for the selective concentration, separation and removal of mixtures of microorganisms.

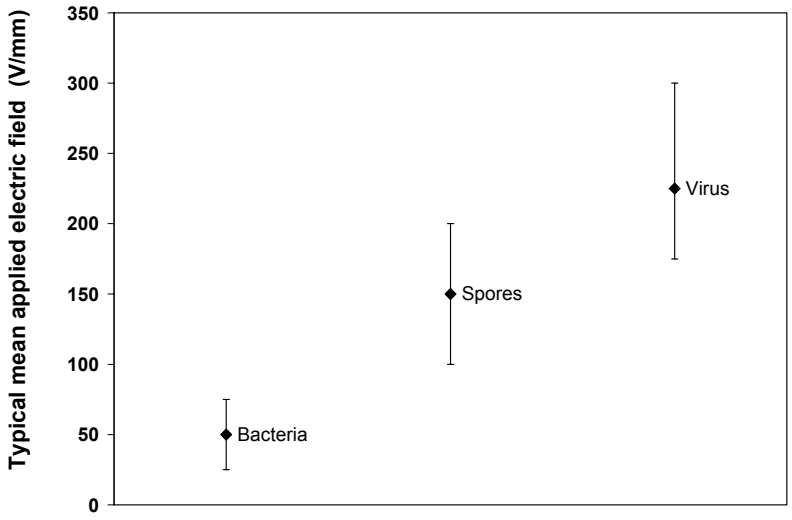

Figure 17. Typical mean applied electric field (in V/mm) required to achieve dielectrophoretic trapping of the three different types of biological particles (bacteria, spore, virus) studied in our system.

3.6 Device Performance: Concentration Factors and Removal Efficiencies

The concentration factor and removal efficiency of the iDEP systems were evaluated by performing experiments where *E. coli* cells with an initial dilution of 1 x 10^5 cells/ml were concentrated and released. The experiments consisted of three parts:

(a) First, a low pressure-driven flow (100 Pa), from the inlet to the outlet, was applied by using custom-made liquid reservoirs at the inlet and outlet of the microchannel; and the number of cells passing through the post-array was evaluated using fluorescence microscopy.

(b) An electric field was applied for a determined period of time (1 or 2 minutes) and the *E. coli* cells were dielectrophoretically trapped in the post-array; the outlet of the post array was observed in order to determine the number of cells that are able to pass through the post-array while the electric field is being applied.

(c) The *E. coli* cells were released from the dielectrophoretic traps as a plug of cells, the concentration of this plug of cells was determined at the outlet of the post array.

For each of these three stages, a 250-frame randomly selected movie was recorded at the outlet of the array. The rate at which particles escape the device while the electric field is applied was estimated by counting the number of cells that pass through the outlet during the 250-frame movie. The number of concentrated cells (plug of cells) achievable was calculated by counting the number of cells in the movie frame with the highest population of cells. By counting the number of cells at these particular instances, removal efficiencies and concentration factors were calculated as follows:

$$RE = \left(\frac{CB - CD}{CB} \right) 100\% \tag{13}$$

$$CF = \frac{CP}{CB} \tag{14}$$

where *RE* is the removal efficiency, *CB* is the rate at which cells flow pass the outlet before the electric field is applied, *CD* is the rate at which cells flow pass the outlet while the electric field is being applied, *CF* is the concentration factor, *CP* is the flow rate of the plug of concentrated cells as they elute the post array.

Figures 18a and 18b show the concentration factor and removal efficiency obtained for *E. coli* cells, respectively. The experimental results depicted in Figure 18 were obtained by applying mean electric fields of 50 V/mm, 75 V/mm, and 100 V/mm for either 1 or 2 minutes. Three experiments were conducted in each configuration for a total of eighteen measurements. Figure 6a shows concentration factors are all above three orders of magnitude. The initial *E. coli* concentration was increased up to 3,200X. Figure 6a shows that the concentration factor increases with the duration of the collection, indicating that the collector has not reached a state of saturation or reached a performance limit in these tests. The concentration factor also increases with increasing applied electric field. These results are expected since, at a given time, the number of cells that have entered the device is proportional to the electric field. Moreover the potential well depth of the dielectrophoretic traps increases with the electric field, so the capacity of the iDEP device increases with increasing field. The concentration factor was measured by counting the particles as they eluted through the post array and it should be noted that the band will become more dispersed further downstream if a pressure driven flow is applied, negatively impacting the measured concentration factor.

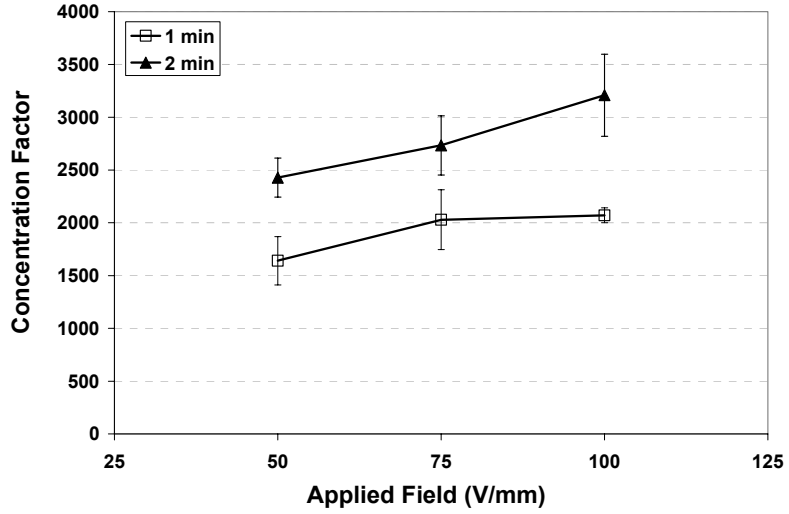

(a)

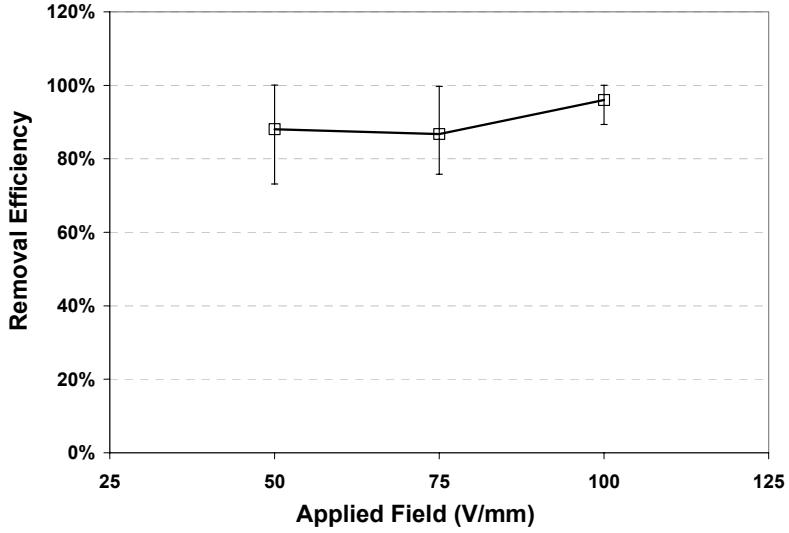

(b)

Figure 18. Results obtained with *E. coli* cells: (a) concentration factor (n=3) and (b) removal efficiency (n=6).

For comparison, Suehiro *et al*. [73] studied a similar system in which dielectric spheres were used as the insulating material to create the nonuniform electric field. A suspension of yeast cells was passed through a chamber containing the insulating spheres, and an electrical field was applied. Cell concentration at the effluent was quantified using a colony counting technique. Suehiro *et al*. reported a concentration factor of 5, a removal efficiency of 99.999%, and recovery efficiency of 70%.

Under the experimental conditions described in this manuscript, the removal efficiency of our micro iDEP device approached 100%. Figure 18b shows the average removal efficiency as a function of the applied electric field. Good removal efficiencies were obtained even at the lowest applied electric field (50 V/mm) since this field is significantly higher than the trapping threshold for *E. coli* cells in our system [74]. Figure 18b shows that the removal efficiency is largely independent of the magnitude of the applied electric field in these experiments. The preliminary results presented in this study were conducted at low initial concentrations to ensure that the experimental conditions were far from saturation to remove particle-to-particle interaction effects and to emulate the particular application we are addressing, water analysis. Future studies will be conducted at varying initial concentrations and in devices operated near saturation, where the removal efficiency should drop precipitously. These experimental results on a prototype concentrator show tremendous promise for iDEP in sample concentration for water analysis.

4. iDEP Device Performance: Polymer

4.1 Feature Characterization: Metrology

Dimensional characterization gives insight to how well the microfluidic structures conform to design specifications. There are a number of reasons to perform dimensional metrology on the stamps and replicates used in this study. The stamp/replicate geometry determines fluid flow characteristics, so understanding the geometry aids in diagnosing performance problems that may arise due to distortions or defects. A quality assessment of the replication process can be made by comparing data from replicates to their corresponding stamp. A comparison between the two etch processes used to pattern the stamp may also be concluded. Moreover, the gathered metrology data provides a baseline for process control and improvement.

White light interferometry was employed to inspect the stamps and replicates used in this research in device fabrication. The Wyko NT3300 surface profiler is a commercially available inspection system equipped with hardware and software for data acquisition and analysis (www.veeco.com). The metrology system has 0.1 nm resolution in the vertical (z) axis. Laterally, in the XY plane, resolution is dependent on the pixel size in each scan. Thus, the objective and field of view of the scan determines lateral resolution. Scans in this study were performed using 20.8x effective magnification, translating to 0.7 μm pixel size. Considering the size scale of the structures involved, this lateral resolution was acceptable. Filters were applied to the scanned data sets to remove tilt so that the desired profilometry could be completed.

The specimens are fabricated using an injection molding process in which the structures are formed on metal stamps using etching processes. The sidewall normality depending on the etch process used. The glass (HF) etching process produces structures that have tapered/sloped sidewall geometries. The Bosch etch creates more of a vertical sidewall; however there are corrugations in the hoop direction from bottom to top of the structures. The size scale of these features is on the order of tens of microns to millimeters laterally and tens to hundreds of microns in height. Dimensional metrology of structures having these characteristic size and topography is challenging. Non-contact profilometry, using a white-light interferometer and the technique utilized, is limited because of signal loss once the topography of the structure exceeds a certain slope. Contact profilometry was avoided because the probe tip must be smaller than the feature size. Also, the stylus must have the necessary clearance to accommodate the slope of the structure's sidewall to avoid interference.

Various measurements were taken to characterize the replication process: post height, surface roughness, vertical range (Top Δz) on the circular post, vertical range (Bottom Δz) on the surrounding surface, and surface area of the circular post. Figure 19 shows a principle sketch of the dimensions measured.

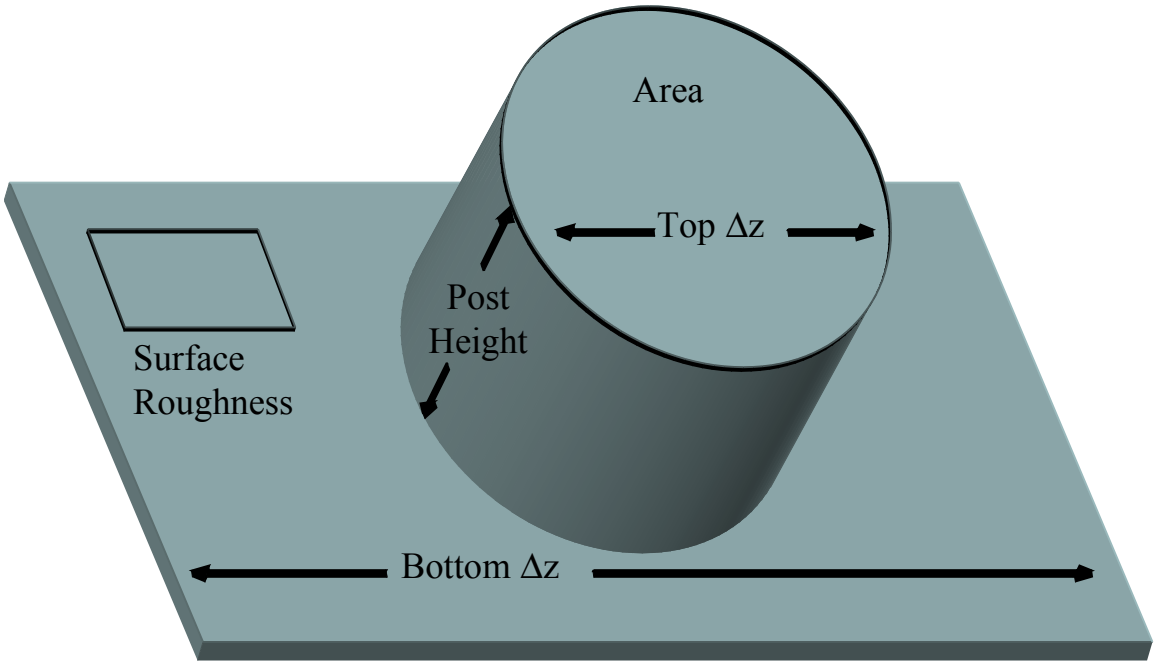

Figure 19. Schematic depiction of metrology measurements of the post structures utilized for comparison.

Data acquired by the interferometer is meaningful despite the signal loss in areas of sloped topography because one goal of this metrology is to compare the stamp to the replicate. If the replication process was ideal, the signal loss seen when inspecting the stamp would transfer over to the plastic replicate. This is the reason for calculating the surface area of the posts. To characterize the replication process, data was taken from an HF glass etched stamp and two of its replicates and a Bosch etched stamp and three of its replicates. Each stamp had similar layouts, consisting of circular posts in rectangular arrays.

The post heights were 55 μm and 75 μm for the wet HF and Bosch etches, respectively. Three posts were chosen on each sample: two 200 μm diameter posts on the 4x10 post pattern and one 150 μm diameter post on the 5x12 post pattern. To guarantee consistency, one objective and field of view setting was chosen based on maximizing the feature size within the field of view across all features inspected. Corresponding posts from stamp to replicate were examined. Figure 20 gives a qualitative perspective on the stamp to replicate quality as well as the repeatability of the replication from both stamp types.

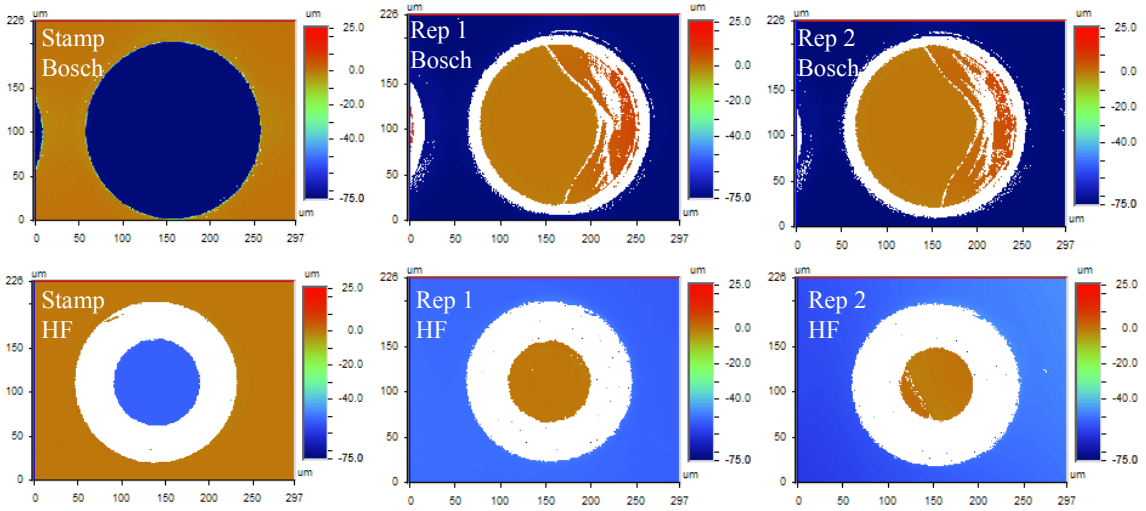

Figure 20. Interferometer data taken of stamp and corresponding replicates for 200 µm diameter posts for Bosch and wet HF replication

Table 3 contains data referring to the nominal design specification, the stamp, the replicate, and the difference between the replicate and the stamp in order to quantify the replication process. The values in Table are expressed as averages across the multiple samples acquired.

Table 3: Replication process measurements

Bosch Etch	Post Height [µm]	Bottom Δz [µm]	Bottom R_a [nm]	Top Δz [µm]	Area[1] [mm^2]	Area[2] [mm^2]
Nominal	75.0	0.0	na	0.0	0.0314	0.0177
Stamp	74.0	1.9	61.1	11.5	0.0320	0.0180
Replicate	74.4	4.3	57.3	12.4	0.0250	0.0097
Replication Δ	0.4	2.4	-3.9	0.9	-0.0070	-0.0083
HF Glass Etch	Post Height [µm]	Bottom Δz [µm]	Bottom R_a [nm]	Top Δz [µm]	Area[1] [mm^2]	Area[2] [mm^2]
Nominal	55.0	0.0	na	0.0	0.0310	0.0177
Stamp	52.8	2.1	34.6	2.6	0.0055	0.0020
Replicate	51.0	2.0	31.6	2.9	0.0063	0.0002
Replication Δ	-1.8	-0.1	-3.0	0.3	0.0008	-0.0018

[1]Area measurement for 200µm diameter posts
[2]Area measurement for 150µm diameter posts

Considering the data presented in Table 3, it is noted that the characteristic post height feature measured replicates to a deviation less than 2 µm from the stamp, indicating good feature fidelity and minimal underfill during the injection molding process. The bottom surfaces of the plastic replicates have minimal differences in height variation and average surface roughness as well, reinforcing this conclusion.

The top surfaces of the replicate posts show small deviations from the stamp as well. There are some observed distortions in the topography of the replicate posts. These distortions are due to the adhesion of the plastic to the metal during release of the replicate from the stamp. The performance of the post pattern is not compromised, because fluids are intended to move around the posts and not over the top surface. The area measurements from nominal-to-stamp and from stamp-to-replicate for the Bosch etch have less variation, meaning less taper than the HF glass etch post structures. To

meet the goals of this research, the posts must have uniform sidewalls as close to vertical as possible. Therefore, the structures formed by the Bosch etch are superior to those created by the HF glass etch. Furthermore, the Bosch etch process is nearest to nominal in post height.

4.2 iDEP Device Performance Characterization

After the devices were characterized by metrology and sealed to form watertight channels, the next step was to evaluate the performance of the devices as a function of fabrication technique. The experimental apparatus utilized is shown in Figure 21.

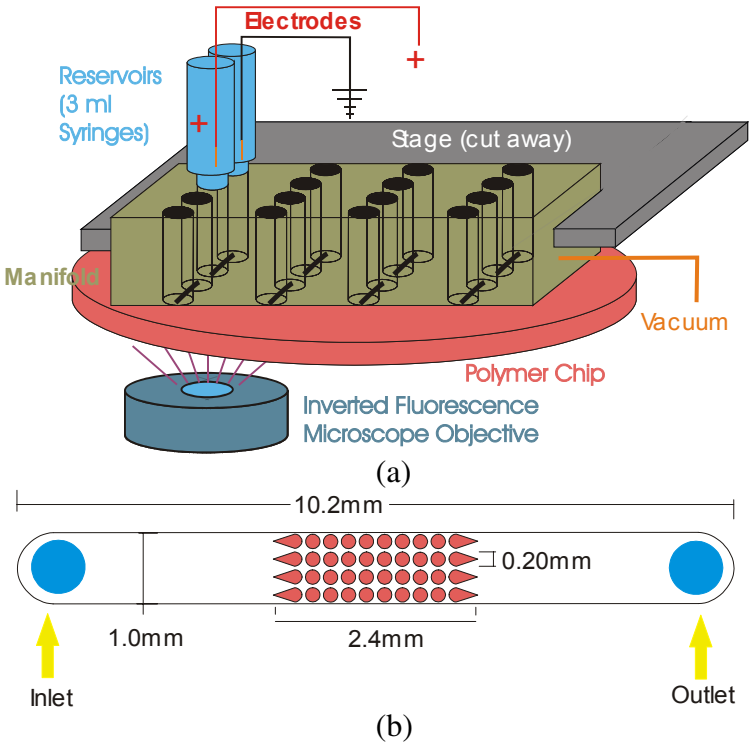

Figure 21. Schematic depiction of the experimental setup showing (a) each device contained 8 individual channels on a chip injection molded from Zeonor® 1060R resin. The chip was sealed to a manifold with a vacuum chuck and the apparatus was clamped to a holder on top of the microscope stage. (b) A schematic of a channel with 4x10 post configuration.

Trapping thresholds were clearly determined by direct observation of particle behavior through epifluorescence microscopy of the microchannels. At a discrete trapping voltage, particles begin to collect in spaces between posts, as seen in figure 22a. This process was found to be highly reversible, with concentrated streams of particles leaving the posts when voltage is discontinued, as shown in figure 22b.

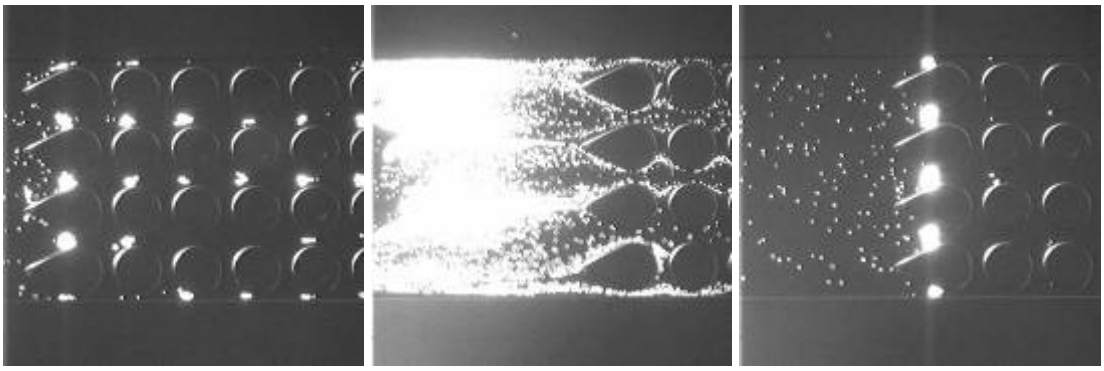

(a) (b) (c)

Figure 22. Stills taken from a movie demonstrating trapping of 2 μm polystyrene beads in an array molded from the Bosch etch-derived polymer iDEP device. Near the trapping threshold (a), array behaves analogously to a packed bed adsorber. Upstream posts saturate and pass particles to traps downstream, creating a saturation wavefront at startup. When the trapping voltage is turned off (b), particles flow out of traps in a concentrated plug. At higher trapping voltages (c), trapped particles remain in the forward posts.

Differential separations based on type of particle were studied in the microchannels formed from the Bosch etch mold. Since the local maxima of the electric field are located in the narrowest region of the gap between posts, particles with a lower trapping threshold will be stopped further away from this region than particles with higher trapping thresholds. At voltages between the trapping thresholds of two tracers, the less readily trapped tracer passed through, while the more readily trapped tracer was retained in the posts. It was observed that 2 μm polystyrene beads were separated from 1 μm and 500 nm polystyrene beads, as shown in Figure 23.

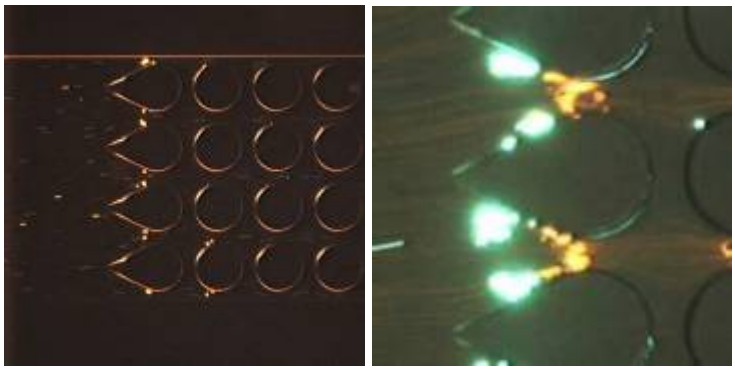

(a) (b)

Figure 23. Demonstration of separation of polystyrene beads by size in a device fabricated through reactive ion etching (Bosch). In (a), 2 μm red beads trap at 50V/mm, while 1 μm green beads pass between posts. (b) At 125V/mm, 2 μm green beads trap further upstream than 500 nm red beads.

Different types of biological tracers were also separated from each other and from non-biological backgrounds and presented in Figure 24. *B. subtilis* spores were separated from 1 μm polystyrene beads. Additionally, to show device operation and selectivity in the presence of an inert background, *B. subtilis* spores were separated from a dense background of 20nm polystyrene beads. *B. subtilis* spores and vegetative cells formed separate bands of trapping at 170 V/mm. Finally, *B. subtilis* and *B. thuringiensis* spores were separated into bands at 200 V/mm. Surprisingly, the trapped *B. thuringiensis* formed the inner band in this separation. *B. thuringensis* spores are slightly larger on average than *B. subtilis* spore, so one would expect them to form the outer band based on size alone. This emphasizes the importance of factors such as particle composition and morphology in determining trapping threshold.

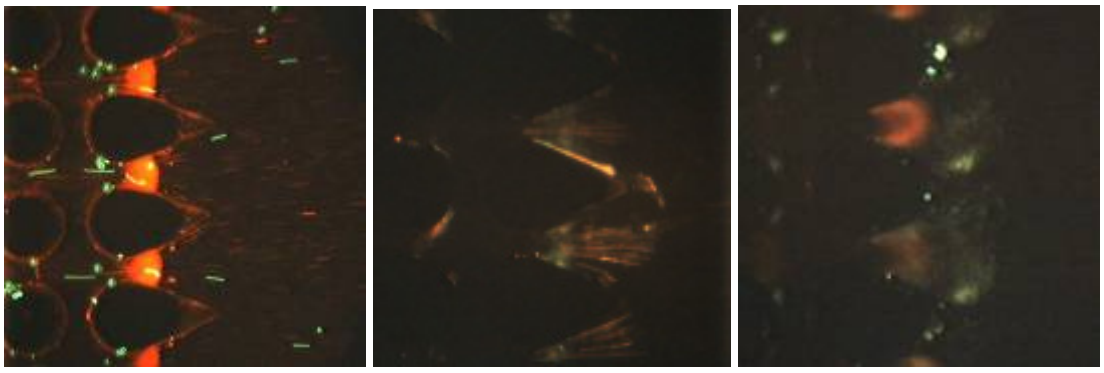

(a) (b) (c)

Figure 24. Differential trapping comparison of biological particles. (a) Red labeled *B. thuringiensis* spores trap between posts at 72 V/mm while 1 μm green polystyrene beads pass through. (b) Differential banding of red labeled vegetative *B. subtilis* cells and green labeled *B. subtilis* spores at 170 V/mm. (c) Differential banding of green labeled *B. subtilis* spores and red labeled *B. thuringiensis* spores at 200 V/mm.

The trapping thresholds for the individual tracer types was found to scale roughly as expected, with particle trapping threshold decreasing with increasing particle size. A major exception to this trend is that biological particles appear to trap more easily than polystyrene beads of comparable size. Vegetative *B. subtilis* cells trapped at a lower threshold voltage than 2 μm polystyrene beads despite having a smaller internal volume than the beads. Otherwise, the order of trapping threshold by increasing voltage was 2 μm beads, *B. subtilis* spores, and 200 nm beads, which corresponds to the relative tracer sizes. In a qualitative study *B. subtilis* spores were observed to trap more readily than 1 μm polystyrene beads, despite having a smaller average size than the 1 μm beads. This is likely due to the high resistivity of the spore coat, when compared with the resistivity of the polystyrene beads. A summary of the trapping thresholds determined for both device types is presented in Figure 25.

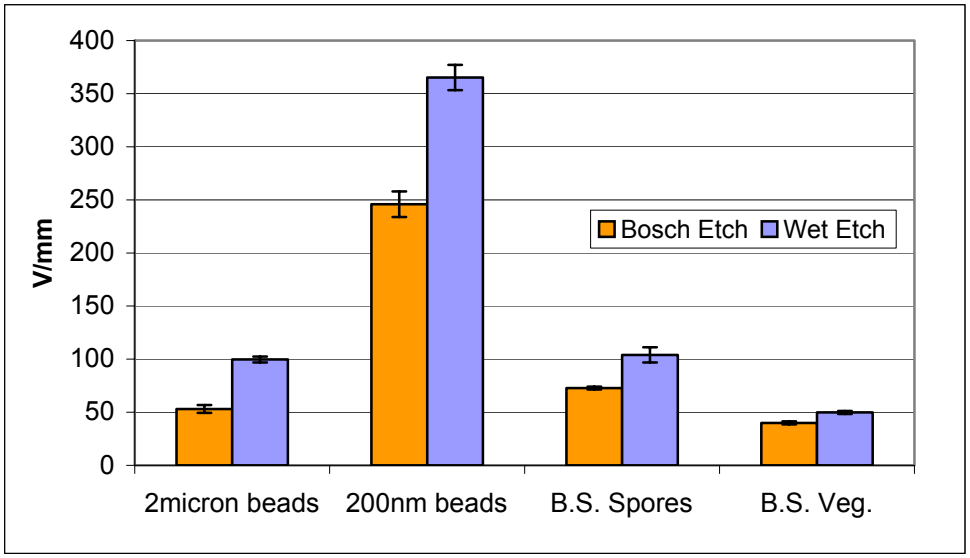

Figure 25. Trapping thresholds of particles studied as a function of fabrication technique. Note that trapping threshold is a function of particle size, conductivity, and morphology.

The trends in the experimentally observed trapping thresholds agree well with expectation based on previous work in glass microchannels. Particles trap at lower voltages in microchannels molded with the stamp made from the Bosch etch master. Conversely, particles require higher voltages to trap in microchannels molded with the stamp made from the HF etch master. The ratio of the trapping voltages for the Bosch and wet etch cases is between 0.54 and 0.79. This may be a function of particle composition or shape, since the ratios observed for the 2 μm and 200 nm spheres are nearly identical.

4.3 Computational Modeling Comparison of Polymer Device Performance Based on Fabrication Technique

After the trapping thresholds of the device were determined experimentally, we proceeded to evaluate the device performance based on rigorous computational modeling algorithms as a means of comparison of real and expected trapping threshold values. Calculations were carried out for the relative trapping performances of the Bosch and HF channels. This required the calculation of the electric fields in each of the channels and using them to calculate trajectories of particles driven by a combination of electroosmosis, electrophoresis and dielectrophoresis.

The liquids of interest here are electrically neutral except for the Debye layers next to the channel walls. Since Debye layers on microchannel walls are usually thin (10 nm) compared to lateral channel dimensions (50 mm), the electric potential, ϕ, satisfies the Laplace equation. In terms of the dimensionless electric potential, $\phi^* = \phi/\Delta\phi$, where $\Delta\phi$ is the potential difference applied across the channel, this is given as Equation 15,

$$\nabla^2 \phi^* = 0, \qquad (15)$$

where the operator is assumed to be dimensionless. The dimensionless electric field, $\boldsymbol{E}^* = \boldsymbol{E}L/\Delta\phi$, is obtained from the electric potential as $\boldsymbol{E}^* = \nabla\phi^*$, where $\boldsymbol{E}$ is the dimensional electric field and L is the length of the channel. Equation 1 shows that for a given geometry there is only one solution for ϕ^*, i.e. there are no parameters. Solutions for the dimensional variables, ϕ and $\boldsymbol{E}$, for specific values of $\Delta\phi$ and L can be obtained from the lone solution for ϕ^* by simply multiplying it, and its gradient, by $\Delta\phi$ and $\Delta\phi /L$, respectively.

Particle trajectories are determined by a combination of fluid flow, electrophoresis and dielectrophoresis. The fluid flow is driven by electroosmosis for the case of interest here. For the thin Debye layer approximation, electroosmotic flow may be simply modeled with a slip velocity adjacent to the channel walls that is proportional to the tangential component of the local electric field, as shown by the Helmholtz-Smoluchowski equation. Here the proportionality constant between the velocity and field is called the electroosmotic mobility, μ_{EO}. Fluid flow in microchannels becomes even simpler for ideal flow conditions where the zeta potential, and hence μ_{EO}, is uniform over all walls and where there are no pressure gradients. For these conditions it can be shown that the fluid velocity at all points in the fluid domain is given by the product of the local electric field and μ_{EO}.

In general, particle velocities can differ from fluid velocities due to electrophoretic and dielectrophoretic forces. The particle velocity induced by electrophoresis, relative to the fluid velocity, is given by the product of the electric field and the electrophoretic mobility, μ_{EP}. Similarly, the dielectrophoretic induced particle velocity is given by the product of the gradient of the electric field squared, $\nabla(\boldsymbol{E}\cdot\boldsymbol{E})$, with the dielectrophetic mobility, μ_{DEP}. The total particle velocity is given by the sum of all of these terms as shown by Equation 16,

$$\boldsymbol{v}_{particle} = \mu_{EK}\boldsymbol{E} + \mu_{DEP}\nabla(\boldsymbol{E}\cdot\boldsymbol{E}) \qquad (16)$$

where the electrokinetic mobility is defined as, $\mu_{EK} = \mu_{EP} + \mu_{EO}$. The mobilities, μ_{DEP} and μ_{EP}, depend on characteristics of the particle and surrounding fluid. Here, we are interested in predicting the ratio of threshold electric potentials, $\Delta\phi_{th}$, that must be applied to the Bosch and HF channels in order to trap various particles. For this it is not necessary to find values for the mobilities, as described below.

A particle is trapped when it is driven into a region where the dielectrophoretic and electrokinetic forces balance and the particle velocity goes to zero. Equation 2 shows that this balance depends on $\boldsymbol{E}$, μ_{DEP} and μ_{EK}. Scaling Equation 16 by $\mu_{EK}\Delta\phi /L$ such that it becomes dimensionless yields Equation 17,

$$\boldsymbol{v}^*_{particle} = \boldsymbol{E}^* + S\nabla(\boldsymbol{E}^*\cdot\boldsymbol{E}^*), \qquad (17)$$

where $S = \Delta\phi\mu_{DEP}/(L^2\mu_{EK})$, which is a dimensionless measure of the relative importance of dielectrophoresis and electrokinesis. Low values of S result in insufficient dielectrophoretic forces to trap particles. There is a threshold value for S, S_{th}, that results in a dielectrophoretic force just large enough to counter the electrokinetic forces. The corresponding threshold value of $\Delta\phi$ can be obtained from S_{th} as $\Delta\phi_{th} = (L^2\mu_{EK}/\mu_{DEP})S_{th}$. Here we are interested in the ratio of values of $\Delta\phi_{th}$ for the Bosch and HF channels, which is given by $\Delta\phi_{th\text{-}Bosch}/\Delta\phi_{th\text{-}HF} = S_{th\text{-}Bosch}/ S_{th\text{-}HF}$, since L, μ_{EK}, and μ_{DEP} are the same for both channels for a given particle type. Particle trajectory calculations were carried out to identify values for S_{th} based on Equation 3 using the solutions for $\boldsymbol{E}^*$ obtained for the Bosch etched and HF etched geometries. Note that only particles that experience negative dielectrophoresis are considered here, i.e. $\mu_{DEP} < 0$, where the dielectrophoretic force acts to drive particles away from regions of large field intensity.

Due to the complex geometries considered here Equation 15 is solved using the finite element method. The finite element meshes for the HF and Bosch channels are shown in Figure 26 where only half of each channel is included due to symmetry. The boundary conditions are, $\phi^* = 1$ at $x/L = x^* = 0$, and $\phi^* = 0$ at $x^* = 1$, and $\nabla\phi^* \cdot \boldsymbol{n} = 0$ over all other surfaces, where $\boldsymbol{n}$ is the local unit vector normal to the surface. The solution for ϕ^* must be differentiated twice to get the dielectrophoretic force on a particle. Consequently, in order to obtain smooth results for this force it was necessary to use a very fine mesh. The meshes shown in Figure 26 contain over one million elements.

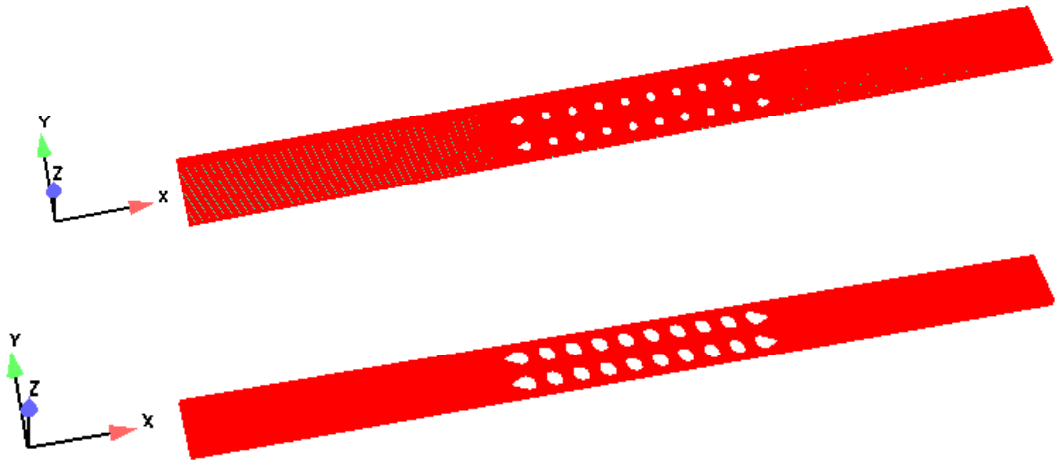

Figure 26. The finite element meshes of the HF (upper) and Bosch (lower) iDEP channels.

Figure 27 shows the solution for the electric potential along the longitudinal centerline. There are three distinct regions in the solution, the post array region, the open region of the channel leading up to the post array region, and another open region leading away from the array region. The gradient in ϕ^* is the largest within the array region due to the restrictions in channel cross section provided by the posts. The gradient is larger for the Bosch channel than the HF channel because of the vertical side walls in the former which results in a smaller open cross section. This results in larger values for $\boldsymbol{E}^*$ and $\nabla(\boldsymbol{E}^*\cdot\boldsymbol{E}^*)$, and is the primary cause of differences in trapping performance between the two channels.

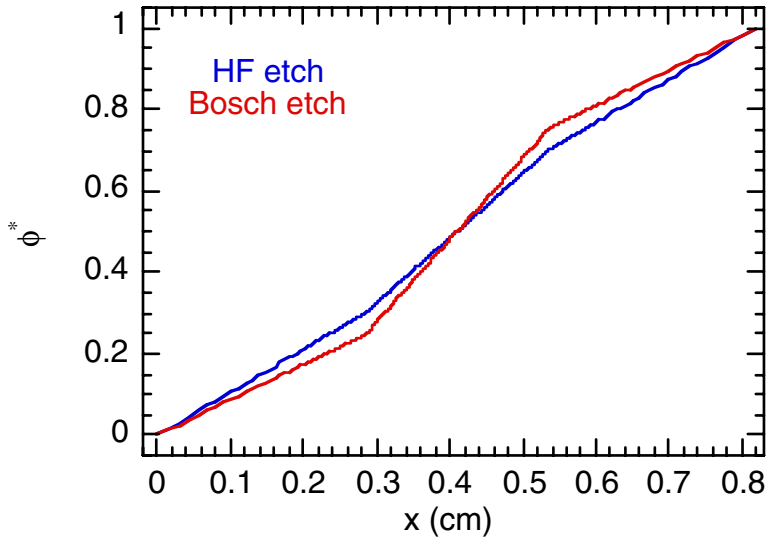

Figure 27. The non-dimensional electric potential as a function of distance along the longitudinal centerlines of the Bosch and HF channels.

Figure 28 shows the x-component of the non-dimensional electric field, $\boldsymbol{E}^*$, in the leading region of the post array. The larger field strength between the posts in the Bosch channel can be seen clearly.

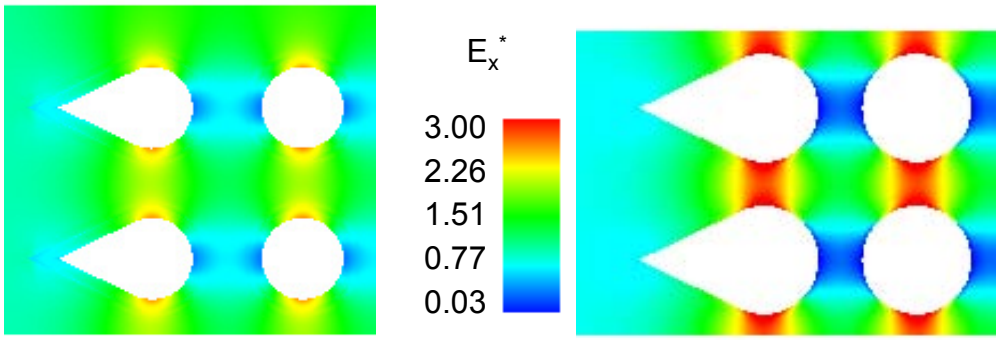

Figure 28. The x-component of the non-dimensional electric field in the leading region of the post array for the HF (left) and Bosch (right) channels.

The x-component of the gradient of the electric field intensity, $\nabla(\boldsymbol{E}^* \cdot \boldsymbol{E}^*)_x$, is shown in Figure 29. Larger values exist between the posts for the Bosch channel compared to the HF channel due to the tighter restrictions between channels in the former, as discussed above for the electric field.

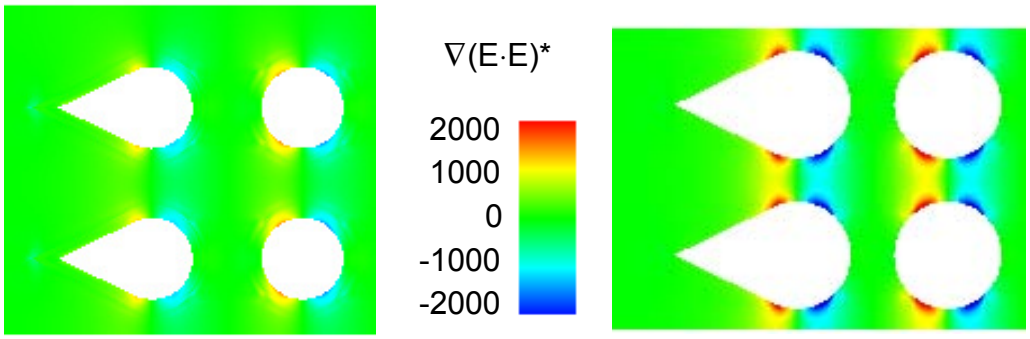

Figure 29. The x-component of the non-dimensional gradient of the electric field intensity in the leading region of the post array for the HF (left) and Bosch (right) channels.

Figure 30 shows the distributions of $\boldsymbol{E}^*_x$ and $\nabla(\boldsymbol{E}^*\cdot\boldsymbol{E}^*)_x$ along a portion of the longitudinal centerline line spanning the leading region of the post array for the Bosch and HF channels. Both $\boldsymbol{E}^*_x$ and $\nabla(\boldsymbol{E}^*\cdot\boldsymbol{E}^*)_x$ are larger between the posts for the Bosch channel than the HF channel. The first peak value of $\nabla(\boldsymbol{E}^*\cdot\boldsymbol{E}^*)_x$ is slightly smaller than the second peak value, corresponding to the teardrop shaped posts and the first row of circular posts, respectively.

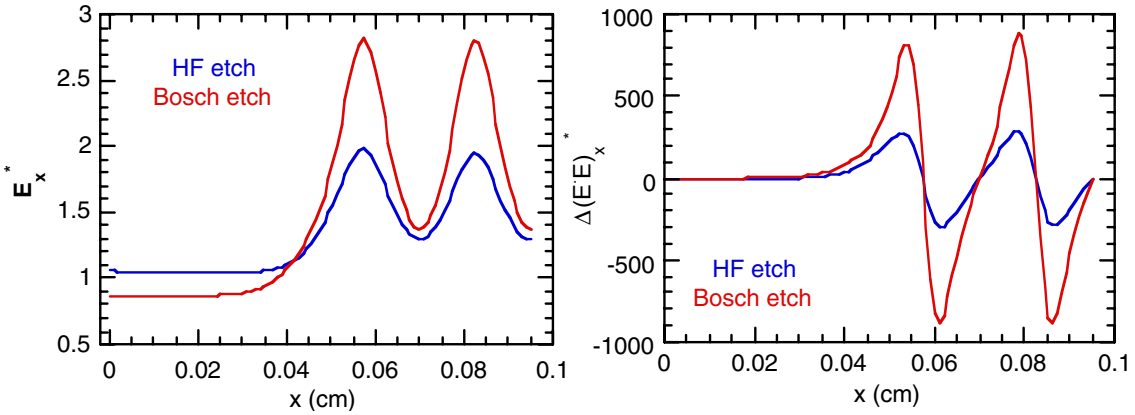

Figure 30. The x-component of the non-dimensional electric field (left) and gradient of the electric field intensity (right) as functions of distance along the longitudinal centerline spanning the leading region of the post array for the HF and Bosch channels.

Particle trajectory calculations were carried out using Equation 17 and the solutions for the electric field presented above. Values of S_{th} were found for each channel that corresponded to their trapping thresholds. Particles were evenly distributed over the inlet to the channels to start the calculations. Results for particle trajectories corresponding to the trapping threshold are shown in Figure 31. The particles are driven away from the posts, for the most part, and are trapped between the posts. Most of the particles are able

to pass the 'teardrop' shaped posts and are trapped at the first row of circular posts where the dielectrophoretic force is larger. Particles are able to completely pass the post array in the HF channel along the outer region of the post array due to the relatively wide open path available there. These particles were not included when determining trapping threshold.

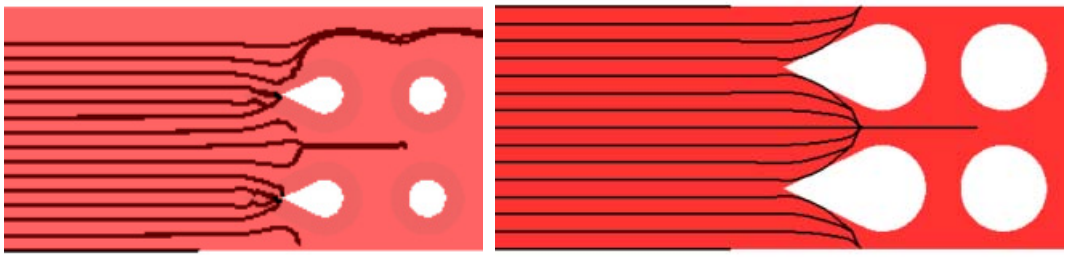

Figure 31. Particle trajectories corresponding to the trapping threshold for the HF (left) and Bosch (right) channels.

Figure 32 shows a transverse channel perspective of several particle trajectories within the channels. This figure gives a clear view of the differences in geometry of the two channels.

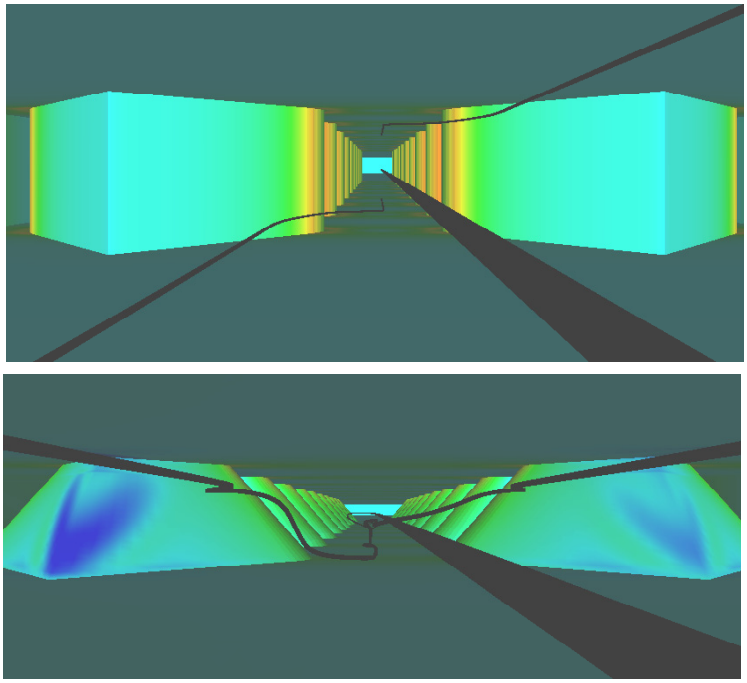

Figure 32. Particle trajectories, shown in black, as seen by particles within the channels, corresponding to the trapping threshold for the Bosch (upper) and HF (lower) channels.

Estimates were made for the mobility values for the particles based on measurements of the electrokinetic flow velocity observed in regions of the channel remote from the post array (μ_{EK} = 0.00023 cm^2/s-V), and the threshold trapping voltage measured for spores (μ_{DEP} = 1.38·10^{-9} cm^4/s-V^2). These were used to calculate dimensional values for the particle velocity, including the individual contributions from electrokinesis and dielectrophoresis. These are shown in Figure 33 as functions of distance along the longitudinal centerline spanning the leading portion of the post array, and in Figure 34 as functions of distance along a lateral line at the location of particle trapping at the first row of circular posts. Due to the smaller value of $\nabla(\boldsymbol{E}^*\cdot\boldsymbol{E}^*)_x$ for the HF channel, a larger electric potential difference is required to trap the particles than for the Bosch channel. The electrokinetic (EK) and dielectrophoretic (DEP) contributions to the particle velocities are different for the Bosch and HF channels, but at the location where the particles are trapped the two contributions add up to zero (the total velocity) for both channels. The plot on the right side of Figure 34 shows the lateral distribution of the particle velocities. This shows that the total velocity is negative everywhere at the longitudinal location of the trapped particles, except at the midpoint between the posts where it is zero. Thus, the weakest part of the trap is at this midpoint.

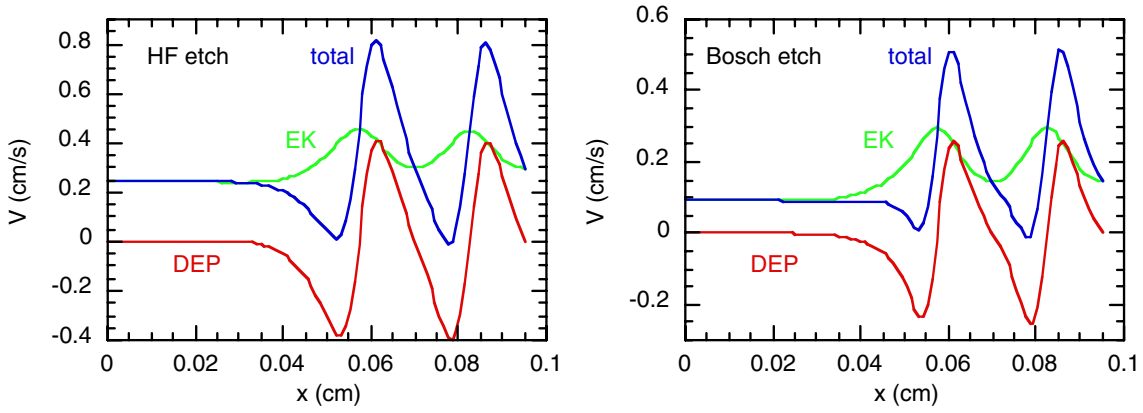

Figure 33. Total, electrokinetic and dielectrophoretic contributions to the particle velocities as functions of distance along the longitudinal centerline spanning the leading portion of the post array for the HF (left) and Bosch (right) channels.

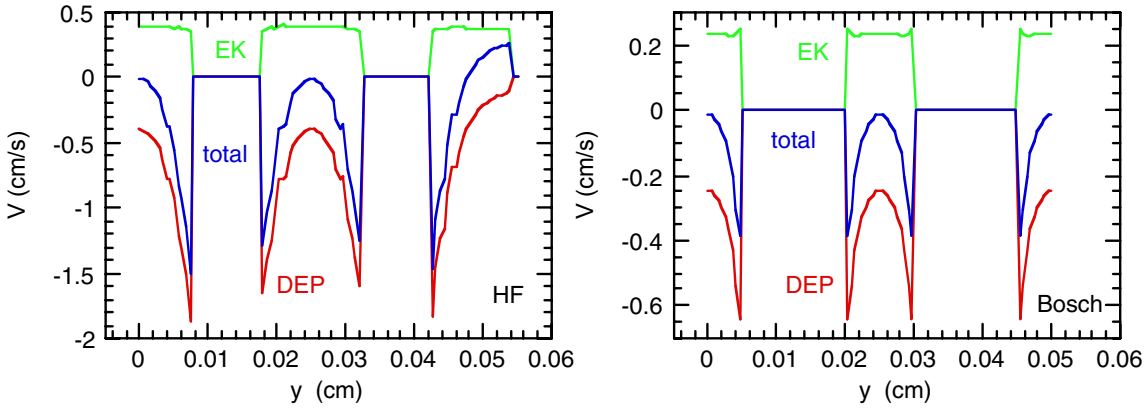

Figure 34. Total, electrokinetic and dielectrophoretic contributions to the particle velocities as functions of distance along the lateral line at the location of particle trapping at the first row of circular posts for the HF (left) and Bosch (right) channels.

Figure 35 shows the ratio of the threshold trapping electric potential differences for the Bosch and HF channels obtained from the calculations along with the experimental values obtained for a number of different particle types. The calculated value of 0.46 is in reasonable agreement with that measured for spores, but the values for the other types of particles are much larger.

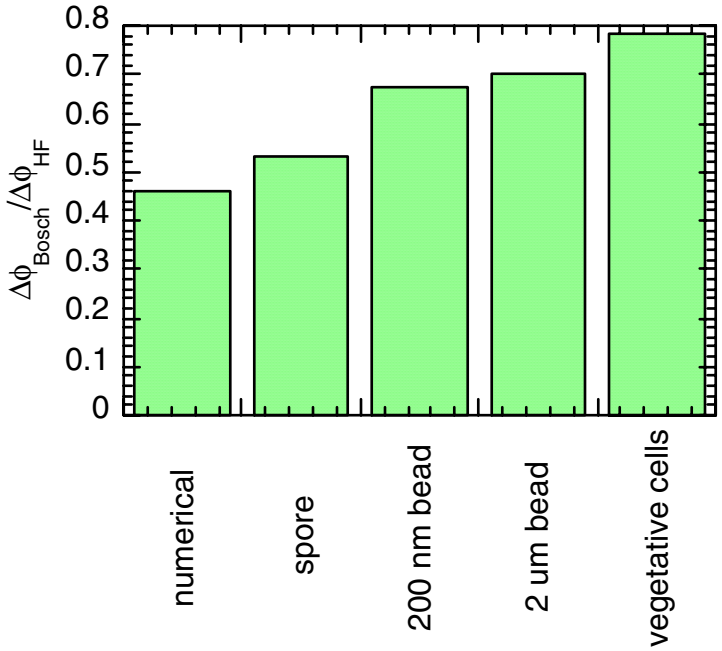

Figure 35. The ratio of the threshold trapping electric potential differences for the Bosch and HF channels as obtained from the calculations and as measured for several different types of particles.

One possible explanation for this difference between the experimental and theoretical values for the ratio of threshold trapping potentials is the presence of particle-particle interactions that may perturb the electric field gradient present between the posts. The local perturbation to the field created by one particle may amplify the dielectrophoretic force acting on a nearby particle. A large number of such interactions may cascade resulting in a significant enhancement of the dielectrophoretic force. This could result in direct contact between particles and van der Waals forces would then act to keep the particle ensemble together.

5. Conclusions

The application of Insulator-Based Dielectrophoresis (iDEP) for the manipulation of bacteria and inert particles has been demonstrated in both glass and polymer devices. Differential dielectrophoretic trapping of live *E. coli* in the presence of dead *E. coli* and inert polystyrene particles was demonstrated in glass iDEP devices. Live *E. coli* exhibited negative dielectrophoretic behavior, i.e., they trapped in regions of lower field intensity. Concentration of *E. coli* was qualitatively observed as result of the cells trapping under the applied electric field. Inert 1-μm polystyrene particles exhibited positive DEP behavior, as they were immobilized in regions of higher field intensity. Differential trapping of 1-μm particles and live *E. coli* was observed. Under the current operating conditions it was not possible to trap 200-nm particles, since due their smaller size, higher DEP force is needed to achieve DEP trapping. When applying iDEP to a mixture of live and dead *E. coli*, it was observed that dead cells are less negatively dielectrophoretic than live cells since dead cells have a more conductive cell membrane than live cells.

Four types of bacteria (*E. coli, B. subtilis, B. cereus,* and *B. megaterium*) exhibited negative dielectrophoretic behavior, i.e., the bacteria were trapped in areas upstream of the peak electric field concentration. The threshold applied electric field required to trap each bacterial species was different for each species. The order of trapping, from lower to higher electric field threshold was: *E coli* < *B. megaterium* < *B. subtilis* < *B. cereus* in both single-bacteria and mixed-bacteria experiments. It was demonstrated that the membrane conductivity is not the parameter controlling the differences in DEP behavior of the cells. Therefore other factors or parameters such as cell size, cell shape and other morphological characteristics are responsible for differences in the dielectrophoretic response of the bacteria. Further investigations of these geometrical effects on the DEP response are needed to be able to predict trapping thresholds and understand what limits exist for the specificity of DC DEP.

Selective trapping was demonstrated when mixtures of two bacterial species were introduced into the glass microchannel. At lower applied electric fields, it was possible to trap one of the bacterial species selectively. At a higher applied electric field, it was possible to trap both bacterial species. Generally, the bacteria were trapped in spatially offset bands that were fully resolved in all but one case. It was possible to separate Gram-negative from Gram-positive bacteria: the Gram-negative *E. coli* had a greater negative dielectrophoretic mobility than the three Gram-positive *Bacillus* species utilized in the study. The dielectrophoretic mobility of the different of *Bacillus* species was observed to be different enough to separate them easily at a DC applied voltage. This selectivity allows concentrating and eluting populations of these cells by concentrating with a high applied electric field, and selectively eluting zones of different cell types by gradually lowering the electric field. The threshold field to trap *B. subtilis* spores was larger than those of vegetative *B. subtilis* cells. This difference allows iDEP devices to separate vegetative cells from spores. The threshold field for trapping tobacco mosaic virus was observed to be larger than those required to trap bacterial cells or spores. Additionally, TMV was selectively concentrated against a background of 200-nm polystyrene particles, demonstrating the ability of iDEP to separate particles having similar sizes.

While glass-based iDEP microdevices perform well, sample throughput is generally low because of the geometrical limitations present in isotropically etched devices. Typical sample flow rates for glass-based devices are in the range of ten microliters per hour. In contrast, polymer-based iDEP devices can be easily scaled to handle much larger sample volumes using commercially available and inexpensive techniques that produce much deeper features and larger channel volumes. Other polymer-based microfluidic devices have been developed and utilized for liquid/liquid and particle separation and other lab-on-a-chip applications including capillary electrophoresis, miniaturized polymerase chain reaction (PCR) chambers, nucleic acid analysis, protein analysis, and fluidic mixers. The main appeal of these polymeric devices is that they are relatively inexpensive and produced employing standard mass fabrication techniques such as injection molding and hot embossing instead of the costly per wafer technique of microlithography. Our group has reported that polymeric iDEP elements can be made from cyclic olefin copolymers such as Zeonor®. Cyclic olefin copolymers (COCs) have received a significant amount of recent interest in microfluidics owing to their low auto-fluorescence and high chemical resistance to a wide range of polar solvents; such properties support the use of this class of polymer for iDEP devices.

Microfluidic devices fabricated from a polymer substrate have been demonstrated to be effective at trapping and concentrating suspended organic particles in flowing water using insulative dielectrophoresis. We have presented here a direct structure-function relationship between the taper of the insulating structures that is dictated by the microfabrication technique. In the present work, microfluidic channels were injection molded from Zeonor® 1060R using two different molds based on the same mask pattern. One mold was electroplated onto an isotropically etched master, while the other mold was electroplated onto a master produced by with anisotropic etch process. The isotropic etch (HF) produced features with a vertical taper, while the anisotropic etch (Bosch) produced features with straight sidewalls. The topography of the resulting devices was thoroughly characterized with metrology and it was found that injection molding reproduced the features of the original masters with a high degree of fidelity.

Sealed microchannels were loaded with different particle suspensions. The minimum DC voltage required to separate each particle type from the surrounding fluid was determined. Significantly higher voltages were required to separate particles in microchannels with tapered (HF) features than in microchannels with straight-walled (Bosch) features. Differential separation of multiple particle types was qualitatively demonstrated. Generally, smaller particles required higher voltage to separate and microorganisms required less voltage to trap than similarly sized polystyrene microspheres. This observed performance was identical to that observed in glass and indicates that the polymer devices are completely amenable to iDEP applications.

The metrology data was used to create a numerical model for the dielectrophoretic devices. The calculated electric field profiles illustrate that non-tapered features are much more effective at creating local variations in field intensity than tapered features. The dynamics of each channel type were studied by the introduction of virtual tracers into the calculated electric field and a ratio of expected threshold voltages required to trap a particle in each channel type was calculated. While the model explained many of the

experimentally observed performance differences between the two different microchannel geometries, there were significant differences between the experimentally observed threshold voltage ratios and the calculated ratio. Both the experimental and modeling studies of iDEP in polymer microchannels strongly suggest that iDEP can be an efficient, selective, and cost effective method for pre-concentrating biological samples for analysis in a microfluidic system. While there remains some disagreement between the theoretical and experimental results presented, the present work clearly illustrates the potential utility of an iDEP device that can isolate and concentrate targeted particles of interest from a diverse background. Such devices may prove useful in the isolation and detection of biological agents for homeland security applications. The results obtained over the course of this project illustrate the great potential of iDEP for the effective concentration of bacteria and particles. An iDEP device can be envisioned as a front-end device for bacterial detection and concentration in water.

Acknowledgments

The authors acknowledge the help and support of Alfredo Morales, John Hachman, Marion Hunter, Karen Krafcik, Renee Shediac, Cindy Harnett, John Brazzle, George Sartor, Susan Jamison, William Kleist, Brian Holliday, Michelle Khine, Jessica Lam, Brita Mittal, and Linda Domeier in the fabrication, assembly, and testing of the glass and polymer chips. The authors thank Judy Rognlien for her assistance in the fluorescent labeling of microorganisms and Allen Salmi for his technical assistance in the fabrication of the chip manifold assembly and electrical safety apparatus.

Distribution

Internal:

1	MS 9292	Y. Fintschenko, 8324
1	MS 9292	B. A. Simmons, 8764
1	MS 9154	R.V. Davalos, 8245
1	MS 9292	G.J. Fiechtner, 8324
1	MS 9035	J.T. Ceremuga, 8243
1	MS 9292	M. Kanouff, 8775
1	MS 9404	A. Pontau, 8750
1	MS 9292	G. Kubiak, 8320
1	MS 9161	W.R. Even, 8760
1	MS 9161	J.L. Lee, 8764
1	MS 1349	W. Einfeld, 6245
1	MS 0701	J. Merson, 6110
1	MS 9004	D. Lindner, 8120
1	MS0123	D. Chavez, LDRD Office, 1011
1	MS0123	H. Westrich, LDRD Office, 1011
2	MS 0899	Technical Library, 4536
2	MS 9018	Central Technical Files, 8945-1

References

1. Pohl, H., *The Motion and Precipitation of Suspensoids in Divergent Electric Fields.* Applied Physics, 1951. **22**: p. 869-871.
2. Jones, T.B., *Electromechanics of Particles*. 1995, USA: Cambridge University Press. 265.
3. Pohl, H., *Some Effects of Nonuniform Fields on Dielectrics.* Applied Physics, 1958. **29**: p. 1182-1188.
4. Crane, J. and H. Pohl, *A study of living and dead yeast cells using dielectrophoresis.* Journal of the Electrochemical Society, 1968. **115**(6): p. 584-586.
5. Betts, W.B., *The potential of dielectrophoresis for the real-time detection of microorganisms in foods.* Trends in Food Science and Technology, 1995. **6**(2): p. 51-58.
6. Cummings, E.B. and A. Singh, *Dielectrophoresis in Microchips Containing Arrays of Insulating Posts: Theoretical and Experimental Results.* Analytical Chemistry, 2003. **75**: p. 4724-4731.
7. Pohl, H. and I. Hawk, *Separation of Living and Dead Cells by Dielectrophoresis.* Science, 1966. **152**(3722): p. 647-649.
8. Pohl, H. and J. Crane, *Dielectrophoresis of Cells.* Biophysical Journal, 1971. **11**(9): p. 711-727.
9. Malyan, B. and W. Balachandran, *Sub-micron sized biological particle manipulation and characterisation.* Journal of Electrostatics, 2001. **51**: p. 15-19.
10. Markx, G.H., et al., *Dielectrophoretic characterization and separation of microorganisms.* Microbiology-UK, 1994. **140**: p. 585-591.
11. Markx, G.H., M.S. Talary, and R. Pethig, *Separation of viable and nonviable yeast using dielectrophoresis.* Journal of Biotechnology, 1994. **32**(1): p. 29-37.
12. Markx, G., P. Dyda, and R. Pethig, *Dielectrophoretic separation of bacteria using a conductivity gradient.* Journal of Biotechnology, 1996. **51**(2): p. 175-180.
13. Medoro, G., et al. *CMOS-only sensors and manipulators for microorganisms*. in *IEDM*. 2000. San Francisco, CA, USA: Proc. IEEE.
14. Medoro, G., et al. *A lab-on-a-chip for cell detection and manipulation*. in *IEEE Sensors*. 2002. Orlando, FL, USA: Proc. IEEE.
15. Medoro, G., et al. *A Lab-on-a-chip for Cell Separation Based on the Moving-Cages Approach*. in *Eurosensors XVI The 16th European Conference on Solid-State Transducers*. 2002. Prague, Czech Republic: Proc. Eurosensors XVI.
16. Müller, T., et al., *A 3-D microelectrode system for handling and caging single cells and particles.* Biosensors and Bioelectronics, 1999. **14**(3): p. 247-256.
17. Fiedler, S., et al., *Dielectrophoretic sorting of particles and cells in a microsystem.* Analytical Chemistry, 1998. **70**(9): p. 1909-1915.
18. Li, H. and R. Bashir, *Dielectrophoretic separation and manipulation of live and heat-treated cells of Listeria on microfabricated devices with interdigitated electrodes.* Sensors and Actuators B-Chemical, 2002. **86**(2-3): p. 215-221.
19. Schnelle, T., et al., *Trapping of viruses in high-frequency electric field cages.* Naturwissenschaften, 1996. **83**(4): p. 172-176.
20. Müller, T., et al., *High frequency electric fields for trapping of viruses.* Biotechnology Techniques, 1996. **10**(4): p. 221-226.
21. Green, N., H. Morgan, and J. Milner, *Manipulation and trapping of sub-micron bioparticles using dielectrophoresis.* Journal of Biochemical and Biophysical Methods, 1997. **35**(2): p. 89-102.
22. Morgan, H. and N. Green, *Dielectrophoretic manipulation of rod-shaped viral particles.* Journal of Electrostatics, 1997. **42**(3): p. 279-293.
23. Morgan, H., M. Hughes, and N. Green, *Separation of submicron bioparticles by dielectrophoresis.* Biophysical Journal, 1999. **77**(1): p. 516-525.
24. Hughes, M., et al., *Manipulation of herpes simplex virus type 1 by dielectrophoresis.* Biochimica et Biophysica Acta-General Subjects, 1998. **1425**(1): p. 119-126.
25. Hughes, M., H. Morgan, and F. Rixon, *Dielectrophoretic manipulation and characterization of herpes simplex virus-1 capsids.* European Biophysics Journal with Biophysics Letters, 2001. **30**(4): p. 268-272.
26. Hughes, M., H. Morgan, and F. Rixon, *Measuring the dielectric properties of herpes simplex virus type 1 virions with dielectrophoresis.* Biochimica et Biophysica Acta-General Subjects, 2002. **1571**(1): p. 1-8.

27. Quinn, C., et al., *Dose-dependent dielectrophoretic response of Cryptosporidium oocysts treated with ozone.* Letters in Applied Microbiology, 1996. **22**(3): p. 224-228.
28. Markx, G., J. Rousselet, and R. Pethig, *DEP-FFF: Field-flow fractionation using non-uniform electric fields.* Journal of Liquid Chromatography & Related Technologies, 1997. **20**(16-17): p. 2857-2872.
29. Pethig, R. and G.H. Markx, *Applications of dielectrophoresis in biotechnology.* Trends in Biotechnology, 1997. **15**(10): p. 426-432.
30. Yang, J., et al., *Cell separation on microfabricated electrodes using dielectrophoretic/gravitational field flow fractionation.* Analytical Chemistry, 1999. **71**(5): p. 911-918.
31. Wang, X.-B., et al., *Cell Separation by Dielectrophoretic Field-flow-fractionation.* Analytical Chemistry, 2000. **72**(4): p. 832-839.
32. Betts, W. and A. Brown, *Dielectrophoretic analysis of microbes in water.* Journal of Applied Microbiology, 1999. **85**: p. 201S-213S.
33. Fuhr, G., et al., *CELL MANIPULATION AND CULTIVATION UNDER AC ELECTRIC-FIELD INFLUENCE IN HIGHLY CONDUCTIVE CULTURE MEDIA.* Biochimica et Biophysica Acta-General Subjects, 1994. **1201**(3): p. 353-360.
34. Gascoyne, P. and J. Vykoukal, *Particle separation by dielectrophoresis.* Electrophoresis, 2002. **23**(13): p. 1973-1983.
35. Markx, G.H. and C.L. Davey, *The dielectric properties of biological cells at radiofrequencies: applications in biotechnology.* Enzyme and Microbial Technology, 1999. **25**(3-5): p. 161-171.
36. Cummings, E. and A. Singh. *Dielectrophoretic trapping without embedded electrodes*. in *SPIE: Conference on Microfluidic Devices and Systems III*. 2000. Santa Clara, CA: Proc. SPIE.
37. Cummings, E.B. *A Comparison of Theoretical and Experimental Electrokinetic and Dielectrophoretic Flow Fields*. in *32nd AIAA Fluid Dynamics Conference and Exhibit 2002*. 2002. St. Louis, Missouri: Proc. 32nd AIAA.
38. Chou, C., et al., *Electrodeless dielectrophoresis of single- and double-stranded DNA.* Biophysical Journal, 2002. **83**(4): p. 2170-2179.
39. Armstrong, D., et al., *Separating microbes in the manner of molecules. 1. Capillary electrokinetic approaches.* Analytical Chemistry, 1999. **71**(24): p. 5465-5469.
40. Armstrong, D. and L. He, *Determination of cell viability in single or mixed samples using capillary electrophoresis laser-induced fluorescence microfluidic systems.* Analytical Chemistry, 2001. **73**(19): p. 4551-4557.
41. Armstrong, D., et al., *Rapid CE microbial assays for consumer products that contain active bacteria.* FEMS Microbiology Letters, 2001. **194**(1): p. 33-37.
42. Armstrong, D.W., et al., *Mechanistic Aspects in the Generation of Apparent Ultrahigh Efficiencies for Colloidal (Microbial) Electrokinetic Separations.* Analytical Chemistry, 2002. **74**(21): p. 5523-5530.
43. Girod, M. and D.W. Armstrong, *Monitoring the migration behavior of living microorganisms in capillary electrophoresis using laser-induced fluorescence detection with a charge-coupled device imaging system.* Electrophoresis, 2002. **23**(13): p. 2048 - 2056.
44. Schneiderheinze, J.M., et al., *High efficiency separation of microbial aggregates using capillary electrophoresis.* FEMS Microbiology Letters, 2000. **189**(1): p. 39-44.
45. Cabrera, C.R. and P. Yager, *Continuous concentration of bacteria in a microfluidic flow cell using electrokinetic techniques.* Electrophoresis, 2001. **22**(2): p. 355 - 362.
46. Kenndler, E. and D. Blaas, *Capillary electrophoresis of macromolecular biological assemblies: bacteria and viruses.* TRAC-Trends in Analytical Chemistry, 2001. **20**(10): p. 543-551.
47. Buszewski, B., et al., *Separation of bacteria by capillary electrophoresis.* Journal of Separation Science, 2003. **26**(11): p. 1045-1049.
48. Kourkine, I., et al., *Detection of Escherichia coli O157 : H7 bacteria by a combination of immunofluorescent staining and capillary electrophoresis.* Electrophoresis, 2003. **24**(4): p. 655-661.
49. Li, P. and D. Harrison, *Transport, manipulation, and reaction of biological cells on-chip using electrokinetic effects.* Analytical Chemistry, 1997. **69**(8): p. 1564-1568.

50. Pfetsch, A. and T. Welsch, *Determination of the electrophoretic mobility of bacteria and their separation by capillary zone electrophoresis.* Fresenius Journal of Analytical Chemistry, 1997. **359**(2): p. 198-201.
51. Mehrishi, J. and J. Bauer, *Electrophoresis of cells and the biological relevance of surface charge.* Electrophoresis, 2002. **23**(13): p. 1984-1994.
52. Radko, S. and A. Chrambach, *Separation and characterization of sub-mu m- and mu m-sized particles by capillary zone electrophoresis.* Electrophoresis, 2002. **23**(13): p. 1957-1972.
53. Torimura, M., et al., *Surface characterization and on-line activity measurements of microorganisms by capillary zone electrophoresis.* Journal of Chromatography B, 1999. **721**(1): p. 31-37.
54. Sonohara, R., et al., *Difference in surface-properties between escherichia-coli and staphylococcus-aureus as revealed by electrophoretic mobility measurements.* Biophysical Chemistry, 1995. **55**(3): p. 273-277.
55. Glynn, J., et al., *Capillary electrophoresis measurements of electrophoretic mobility for colloidal particles of biological interest.* Applied and Environmental Microbiology, 1998. **64**(7): p. 2572-2577.
56. Armstrong, D.W. and J.M. Schneiderheinze, *Rapid Identification of the Bacterial Pathogens Responsible for Urinary Tract Infections Using Direct Injection CE.* Analytical Chemistry, 2000. **72**(18): p. 4474-4476.
57. Giddings, J.C., *Field-Flow Fractionation: Analysis of Macromolecular, Colloidal, and Particulate Materials.* Science, 1993. **269**: p. 1456-1465.
58. Lee, H., et al., *Analysis of whole bacterial cells by flow field-flow fractionation and matrix-assisted laser desorption/ionization time-of-flight mass spectrometry.* Analytical Chemistry, 2003. **75**(11): p. 2746-2752.
59. Gao, Y.-S., S.C. Lorbach, and R. Blake, *Separation of bacteria by sedimentation field-flow fractionation.* Journal of Microcolumn Separations, 1997. **9**(6): p. 497 - 501.
60. Cummings, E. and A. Singh, *Dielectrophoresis in Microchips Containing Arrays of Insulating Posts: Theoretical and Experimental Results.* Analytical Chemistry, 2003. **75**: p. 4724-4731.
61. Benguigui, L. and I.J. Lin, *Phenomenological Aspect of Particle Trapping by Dielectrophoresis.* Journal of Applied Physics, 1984. **56**: p. 3294-3297.
62. Van den Wal, A., et al., *Conductivity and Dielectric Dispersion of Gram-Positive Bacterial Cells.* Journal of Colloid and Interface Science, 1997. **186**: p. 71-79.
63. Carstensen, E.L., et al., *Passive Electrical Properties of Microorganisms I. Conductivity of Escherichia coli and Micrococcus lysodeikticus.* Biophysical Journal, 1965. **5**: p. 289-300.
64. Carstensen, E.L., *Passive Electrical Properties of Microorganisms II. Resistance of the Bacterial Membrane.* Biophysical Journal, 1967. **7**: p. 493-503.
65. Burt, J., et al., *Dielectrophoretic Characterization of Friend Murine Erythroleukaemic Cells as a Measure of Induced Differentiation.* Biochimica et Biophysica Acta, 1990. **1034**: p. 93-101.
66. Yunus, Z., et al., *A simple method for the measurement of bacterial particle conductivities.* Journal of Microbiological Methods, 2002. **51**(3): p. 401-406.
67. Ausubel, F.M., et al., *Short Protocols in molecular Biology*. 5th ed. 2002, USA: Wiley. 1-6.
68. Green, N. and H. Morgan, *Dielectrophoretic investigations of sub-micrometre latex spheres.* Journal of Physics D: Applied Physics, 1997. **30**(18): p. 2626-2633.
69. Prescott, L.M., J.P. Harley, and D.A. Klein, *Microbiology*. 2nd ed. 1993, Dubuque, IA USA: Wm. C. Brown Publishers. 912.
70. Moat, A.G., J.W. Foster, and M.P. Spector, *Microbial Physiology*. Fourth Edition ed. 2002, New York: Wiley-Liss. 715.
71. Suehiro, J., et al., *Selective detection of viable bacteria using dielectrophoretic impedance measurement method.* Journal of Electrostatics, 2003. **57**(2): p. 157-168.
72. Lapizco-Encinas, B.H., et al., *Dielectrophoretic Concentration and Separation of Live and Dead Bacteria in an Array of Insulators.* Analytical Chemistry, 2004. **76**(6): p. 1571-1579.
73. Suehiro, J., et al. *Dielectrophoretic filter for separation and recovery of biological cells in water*. in *IEEE Annual Meeting of the Industry-Applications-Society*. 2003. Pittsburgh, Pennsylvania: Proc. IEEE.
74. Lapizco-Encinas, B.H., et al., *Insulator-Based Dielectrophoresis for the Selective Concentration and Separation of Live Bacteria in Water.* Electrophoresis, 2004. **25**: p. 1695-1704.